Acta Geochim (2026) 45:65–85
https://doi.org/10.1007/s11631-025-00780-z

ORIGINAL ARTICLE

Heat flow as a catalyst for radiogenic helium release in the East Africa Rift System

Ernest Mulaya[1,2] · Jon Gluyas[2] · Ken McCaffrey[2] · David Byrne[3] · Chris Ballentine[4]

Received: 11 November 2024 / Revised: 20 March 2025 / Accepted: 30 March 2025 / Published online: 23 May 2025

Abstract The Rukwa Rift section of the East Africa Rift System presents a type setting for radiogenic helium accumulation in a petroleum free basin. As a prerequisite for accumulation, a considerable high heat flow anomaly is required from tectonothermal events to drive the release and circulation of radiogenic helium in the continental crust. Here we apply statistical analysis on geochemical data observed in thermal springs and recorded heat flow to account for crustal helium mass balance for each tectonothermal event in the region. Our results demonstrate anomalously high heat flow ~ 64–99 mW/m^2 with a consistent trend of helium isotopic ratio and fluid chemistry in the Rukwa Rift. Mass balance calculation show that the whole crustal volume underlying the East Africa Helium Pool (EAHP) has a capability of producing radiogenic helium of about 9.9×10^6 mol/yr (22×10^{-6} mol ^{4}He/m^2 yr) while the total radiogenic helium flux ranges between ~2.39×10^6 mol/yr and ~2.68×10^9 mol/yr. The Tanzania Craton contributes largely to radiogenic helium releasing up to 50% of the total capacity in the region. The total ^{4}He emission in the Rukwa Rift Basin is about 4.45×10^5–5.01×10^8 mol/yr which is thus equivalent to 19%–21% of the total production capacity in the region. These results imply that the helium accumulation in the EAHP would have started as early as Paleoproterozoic (2.349 Ga). These results provide a qualitative and quantitative insight to assess both helium and geothermal potentiality in the region.

Keywords Radiogenic helium · Rukwa Rift · Heat flow · Helium potential · Helium concentration

1 Introduction

Global supplies of helium have to date been produced as a by-product from natural gas fields. Almost all natural gas accumulations contain traces of helium albeit with different origins that is, organic (natural gas) versus radiogenic/primordial sources (helium) (Ballentine and Lollar 2002; Danabalan 2017; Gluyas 2019a, b; Danabalan et al. 2022). The current global helium reserves occur as a serendipitous discovery from giant natural gas provinces such as US Midwest, Canada, Poland, Qatar, Algeria and Australia (Gluyas 2019a, b). However, the Rukwa Rift in the Tanzanian section of the East African Rift System (EARS) presents a rare setting of a petroleum-free prospect rich in radiogenic helium (Gluyas 2019a, b; Danabalan et al. 2022). The radiogenic helium flux in the Rukwa Rift segments is associated with thermal springs along with nitrogen, carbon dioxide and other noble gases (Barry et al. 2013; Danabalan 2017; Danabalan et al. 2022).

Previous work on the isotopic ratios and gas chemistry from the RRB provide important clues that suggest a binary mixing and degassing model from both mantle and crustal origins (e.g., Barry et al. 2013; Danabalan 2017; Mtili et al. 2021; Kimani et al. 2021; Danabalan et al. 2022). However, like many other active extensional tectonic regions, the RRB shows a wide range of flux rate and chemical variability

✉ Ernest Mulaya
ernestmulaya@gmail.com

[1] School of Mines and Geosciences, University of Dar es Salaam, P.O. Box 35052, Dar es Salaam, Tanzania

[2] Department of Earth Sciences, Durham University, Durham DH13LE, UK

[3] Centre de Recherches P´etrographiques et G´Eochimiques, UMR 7358 CNRS—Universit´e de Lorraine, BP 20, 54501 Vandoeuvre-l`es-Nancy, France

[4] Department of Earth Sciences, University of Oxford, Oxford OX13AN, UK

associated with potentially high thermal anomalies (Lowenstern et al. 2014; Danabalan et al. 2022; Didas et al. 2022). Although the release of crustal helium depends largely on thermal conditions (e.g., Danabalan et al. 2022), the distribution of the heat flow anomaly in relation to the helium potential in the RRB remains poorly understood.

In this contribution the mass balance between ^{4}He efflux and production potential of each particular tectonic setting/terrane are quantified in the region which we name the East Africa Helium Pool (EAHP) (Fig. 1A, B). We account for ^{4}He production capacity of crustal volumes and flux rate through concentrations observed in thermal springs from previous studies in the RRB (e.g., Barry et al. 2013; Lee et al. 2016; Mtili et al. 2021). The calculations assume that each tectonothermal event recorded in the RRB was associated with a heat flow surge (e.g., Torgersen 2010; Lowenstern et al. 2014). The heat flow affects the primary release of radiogenic helium from helium-retentive minerals such as apatite, zircon, and uraninite and initiate diffusive transport (Danabalan et al. 2022). This study provides insights into the timescale of helium production, release and a possible timing of accumulation surge triggered by heat flow anomaly.

2 Geological background

2.1 Geology and tectonic settings

The tectonics setting and terranes that underlie the EAHP comprises the Tanzania Craton, the Bangweulu Craton and the Ubendian mobile belt (Fig. 1A, B). These terranes surround the RRB and influenced its development (Boniface 2009; Boniface and Schenk 2012; Fig. 1A, B). The Tanzania and Bangweulu cratons comprises mainly granitoids and metamorphic rocks such as granitic gneisses and migmatites (Andersen and Unrug 1984; Manya et al. 2007).

The Ubendian mobile belt consists of uplifted Palaeoproterozoic rocks composed of amphiboles-granulite metamorphic facies (Boniface and Schenk 2012; Fritz et al. 2013). The Ubendian mobile belt is divided into eight Palaeproterozoic terranes which include; Kate-Kipili, Mbozi, Katuma, Ufipa, Wakole, Ubende, Upangwa and Lupa terranes (Daly 1988; Lenoir et al. 1994; Theunissen et al. 1996; Fig. 1A, B).

The EAHP behaves as a comprehensive closed system comprised of rocks which are rich in helium bearing minerals that is, uranium and thorium bearing minerals with average crustal density and thickness of ~2.7 g/cc and 42 km respectively (Adams et al 1959; Burwash and Cumming 1976; Chaki et al. 2008; René 2017; Lavayssière et al. 2019). The uranium concentration in both Tanzania and Bangweulu cratons is ~18.7 ppm, which is 6–7 times, above the average concentration ~2.8 ppm recorded over other Precambrian terranes (Manya et al. 2007; Mshiu and Maboko 2012). The thorium concentrations are 5 times higher in the cratons (~52.1 ppm) than in other Precambrian terranes (~10.7 ppm) (Manya et al. 2007; Mshiu and Maboko 2012).

2.2 Tectonothermal events

Several regional tectonothermal events have been previously mapped in the EAHP (e.g.Ebinger et al. 1989; Kilembe and Rosendahl 1992; Mulaya et al. 2022). Notably, the orogenic

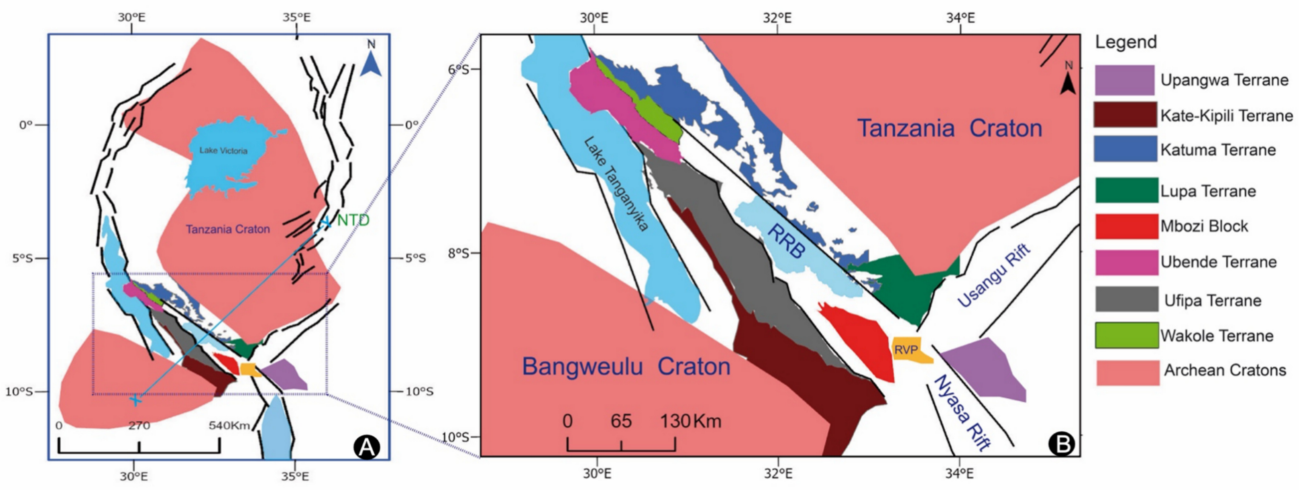

Fig. 1 (A) Map showing tectonic terranes which we refer as East Africa Helium Pool (EAHP). (B) Map showing the tectonic terranes surrounding the Rukwa Rift within the Ubendian mobile belt. RRB. Rukwa Rift Basin, RVP. Rukwa Volcanic Province, NTD. North Tanzanian Divergence

event which led to the Ubendian mobile belt dates back to 500 Ma (Tanganyika Orogeny) which involved a collision between the Tanzania Craton and the Bangweulu Craton (Quennell et al. 1956; Lenoir et al. 1994; Boniface 2009). At least three rifting episodes have been identified in the RRB and Rungwe Volcanic Province (RVP) including Karoo rifting (Late Carboniferous to Triassic), Cretaceous to Oligocene rifting and the Cenozoic rifting (Late Miocene to present) (Ebinger et al. 1989; Kilembe and Rosendahl 1992; Ebinger and Sleep 1998; Delvaux 2001; Boniface 2017; Mulaya et al. 2022). These events as in many other similar tectonic settings (e.g., Lowernstern et al. 2014) are associated with rifting, orogeny and volcanic activity (Danabalan et al. 2022). All these events were likely associated with heat flow surges that can facilitate fluid mobilization and helium degassing in the active tectonic setting of the RRB (Lowernstern et al. 2014; Danabalan et al. 2022).

3 Methodology

3.1 Defining a closed system for helium production and release

Geochemical and isotope data used in this study were compiled by James (1967); Barry et al. (2013); Mtili et al. (2021); Kimani et al. (2021) and the mass balance computation (Tables 1, 2) follows methods described by Lowenstern et al. (2014). These data were used to compute for helium flux and production models by assuming a closed system where fluids interact mainly in rocks within the tectonic terranes surrounding the RRB (e.g., Lowenstern et al. 2014). The closed system defined in this study is named as the EAHP (Figs. 1A, B) whose areas were calculated from ArcGIS Pro shapefiles (Tables 1, 2). The EAHP includes the Ubendian mobile belt ~114,000 km^2, the Bangweulu Craton ~150,000 km^2 (Andersen and Unrug 1984) and the Tanzania Craton ~350,000 km^2 (Danabalan et al. 2022). The EAHP consist of the Ubendian terranes which surround the Rukwa Rift segment of the East Africa Rift System (Fig. 1A, B).

The total calculated helium production rate per year for the whole EAHP is therefore referred as a Whole-Crust (WC) value against which all the helium fluxes in the system were balanced (Table 3). The mass balance computation is based on the fact that ^4He can accumulate over time within the EAHP whereas tectonic activity can facilitate degassing and circulation in the region (Ingebritsen and Manning 2010; Lowenstern et al. 2014; Danabalan et al. 2022).

3.2 Statistical modeling of ^4He mass balance and heat flow anomaly

Two different cases for the helium flux model were considered for the selected closed system boundary (Tables 1 and 2). The choice of parameters for the two cases is based on previously reported CO_2 flux estimates of 4.05 and 0.0055 tonnes/day in areas sized 981.5 and 1500 km^2 respectively (Barry et al. 2013; Lee et al. 2016). Previously, the lowest and highest end member of crustal and mantle Ra signatures have been reported as 0.02 Ra and 8.0 Ra respectively and hence these values were adopted in this study (Barry et al. 2013; Mtili et al. 2021; Danabalan et al. 2022).

Heat flow data were extracted from previous work by Morley et al. (1999), Njinju et al. (2019) and Didas et al. (2022). The few available isotopic ratios, heat flow and geochemical data from previous studies such as $CO_2/^3He$ and R/Ra (Morley et al. 1999; Barry et al. 2013; Danabalan 2017; Njinju et al. 2019; Mtili et al. 2021 and Didas et al. 2022) were used for statistical interpolation across the RRB and RVP using ArcGIS Pro.

For the statistical interpolation in ArcGIS Pro, the Inverse Distance Weighting (IDW) method (Geostatistical Analyst Tool) was applied, using the available isotope ratio (Ra), CO_2 flux and heat flow data as inputs (assuming output cell size ~0.01, power of ~2 and number of points up to 12) to produce raster images. From the raster images of Ra and $CO_2/^3He$ about 1000 random discrete points were created statistically where a number of random points depends on the resolution required to produce reliable neighbourhoods (Fig. 2). These random points surround various locations where data had been previously sampled/computed in the RRB and RVP (Fig. 2). Finally, the cell values from the raster maps were extracted and statistically assigned to those 1000 random points using the Spatial Analyst Tools ('Extract values to points') to represent unique cell values for interpolated Ra and $CO_2/^3He$. The averages of interpolated cell values bounded by each tectonic terrane were used as inputs during mass balance computation (Tables 1, 2).

4 Results

4.1 Heat flow distribution in the Rukwa Rift

The distribution of heat flow data in the Rukwa Rift shows a consistent trend along strike of the Rukwa Rift Basin (RRB) and the Rungwe Volcanic Province (RVP) (Fig. 3A, B). In the RRB the heat flow ranges between 64 mW/m^2 and 86 mW/m^2 above the global average for Mid-Permian Provinces (e.g., Njinju et al. 2019; Fig. 3A, B). The heat flow is higher in the Rungwe Volcanic Province up to 99 mW/m^2 and drops sharply towards the Rukwa Rift graben (minimum 64 mW/

Table 1 Case-I: CO_2 and He flux for the various tectonic settings of the EAHP. Original flux data e.g., CO_2 were extracted from Lee et al. (2016); Barry et al. (2013); Mtili et al. (2021); Danabalan et al. (2022) while other parameters were interpolated using statistical tools in ArcGIS Pro software

Thermal area	Area (km^2)	QCO_2 (grams/day)	CO_2 (mol/yr)	$CO_2/^3He$	$CO_2/^4He$	Q^4He (mol/yr)	R/Ra Mantle^2	R/Ra Local	$^3He/^4He$	$f_{crustal}$	q^CHe (mol/yr)	WC	CO_2 Flux(Mt/yr)	Area of flux
Rukwa Basin	8890	1.01E+11	8.34E+11	5.8E+09	1.6E+03	5.1E+08	8.00E+00	0.2	2.8E−07	9.8E-01	5.01E+08	51	4.05	981.5
RVP	1500	1.70E+10	1.41E+11	8.7E+09	4.0E+04	3.5E+06	8.00E+00	3.3	4.6E−06	5.9E-01	2.07E+06	0		
Ubende Terrane	5275	5.96E+10	4.95E+11	1.0E+10	1.7E+04	2.9E+07	8.00E+00	1.2	1.7E−06	8.5E-01	2.51E+07	3		
Wakole Terrane	2045	2.31E+10	1.92E+11	9.9E+09	1.7E+04	1.2E+07	8.00E+00	1.2	1.7E−06	8.5E-01	9.81E+06	1		
Ufipa Terrane	13,978	1.58E+11	1.31E+12	9.2E+09	1.4E+04	9.2E+07	8.00E+00	1.1	1.5E−06	8.6E-01	7.96E+07	8		
Lupa Terrane	6560	7.42E+10	6.15E+11	7.9E+09	2.1E+04	2.9E+07	8.00E+00	1.9	2.7E−06	7.6E-01	2.22E+07	2		
Nyika Terrane	10,310	1.17E+11	9.67E+11	6.4E+09	3.0E+04	3.2E+07	8.00E+00	3.4	4.8E−06	5.8E-01	1.83E+07	2		
Bangweulu Craton	150,000	1.70E+12	1.41E+13	1.1E+10	1.9E+04	7.2E+08	8.00E+00	1.3	1.8E−06	8.4E-01	6.08E+08	62		
Tanzania Craton	350,000	3.96E+12	3.28E+13	1.0E+10	2.2E+04	1.5E+09	8.00E+00	1.5	2.1E−06	8.1E-01	1.22E+09	124		
Total	614,293.6										2.68E+09	272.06		

Table 2 Case-II: CO_2 and He flux for the various tectonic settings of the EAHP. Original flux data e.g., CO_2 were extracted from Lee et al. (2016); Barry et al. (2013); Mtili et al. (2021); Danabalan et al. (2022) while other parameters were interpolated using statistical tools in ArcGIS Pro software

Thermal area	Area (km^2)	QCO_2 (grams/day)	CO_2 (mol/yr)	$CO_2/^3He$	$CO2/^4He$	Q^4He (mol/yr)	R/Ra $Mantle^2$	R/Ra Local	$^3He/^4He$	$f_{crustal}$	q^CHe (mol/yr)	WC	CO_2 Flux (Mt/yr)	Area of flux
Rukwa Basin	8890	8.93E+07	7.41E+08	5,810,147,238	1.63E+03	4.55E+05	8.00E+00	0.2	0.00000028	9.77E−01	4.45E+05	0.05	0.0055	1500
RVP	1500	1.51E+07	1.25E+08	8,669,586,054	4.01E+04	3.12E+03	8.00E+00	3.3	0.00000462	5.89E−01	1.84E+03	0.00		
Ubende Terrane	5275	5.30E+07	4.39E+08	9,983,714,962	1.68E+04	2.62E+04	8.00E+00	1.2	0.00000168	8.52E−01	2.23E+04	0.00		
Wakole Terrane	2045	2.05E+07	1.70E+08	9,913,632,768	1.67E+04	1.02E+04	8.00E+00	1.2	0.00000168	8.52E−01	8.72E+03	0.00		
Ufipa Terrane	13,978	1.40E+08	1.16E+09	9,247,200,474	1.42E+04	8.18E+04	8.00E+00	1.1	0.00000154	8.65E−01	7.07E+04	0.01		
Lupa Terrane	6560	6.59E+07	5.47E+08	7,947,573,838	2.11E+04	2.59E+04	8.00E+00	1.9	0.00000266	7.64E−01	1.98E+04	0.00		
Katuma Terrane	3883	3.90E+07	3.24E+08	9,577,752,101	1.61E+04	2.01E+04	8.00E+00	1.2	0.00000168	8.52E−01	1.71E+04	0.00		
Upangwa Terrane	11,081	1.11E+08	9.23E+08	2,310,542,513	1.20E+04	7.71E+04	8.00E+00	3.7	0.00000518	5.39E−01	4.16E+04	0.00		
Mbozi Terranes	7887.5	7.92E+07	6.57E+08	21,669,463,904	7.89E+04	8.33E+03	8.00E+00	2.6	0.00000364	6.77E−01	5.64E+03	0.00		
Kate-Kipili Terrane	42,884.1	4.31E+08	3.57E+09	11,611,227,264	2.60E+04	1.37E+05	8.00E+00	1.6	0.00000224	8.02E−01	1.10E+05	0.01		
Nyika Terrane	10,310	1.04E+08	8.59E+08	6,393,470,310	3.04E+04	2.82E+04	8.00E+00	3.4	0.00000476	5.76E−01	1.63E+04	0.00		
Bangweulu Craton	150,000	1.51E+09	1.25E+10	10,672,146,767	1.94E+04	6.43E+05	8.00E+00	1.3	0.00000182	8.40E−01	5.40E+05	0.05		
Tanzania Craton	350,000	3.52E+09	2.92E+10	10,415,137,036	2.19E+04	1.33E+06	8.00E+00	1.5	0.0000021	8.15E−01	1.09E+06	0.11		
Total	114,293.6										2.39E+06	0.24		

Table 3 Radiogenic helium production models. Concentration data sourced from Manya et al. (2007); Chaki et al. (2008); Mshiu and Maboko. (2012); Lavayssière et al. (2019); Danabalan et al. (2022)

Location	U Conc. (ppm)	Th Conc. (ppm)	J^4He Prod (atoms/g/yr)	Crustal ρ g/cc	Total Area (cm^2)	Thickness (cm)	Mass (g)	Mass/NA (gmol)	Q^C4He ($molyr^{-1}$)
Cratons	18.7	52.1	1.0E + 08	2.7	5.0E + 15	4.2E + 06	5.67E + 22	9.4E−02	9.5E + 06
Other terranes	2.8	10.7	1.7E + 07	2.7	1.1E + 15	4.2E + 06	1.29609E + 22	2.2E−02	3.7E + 05

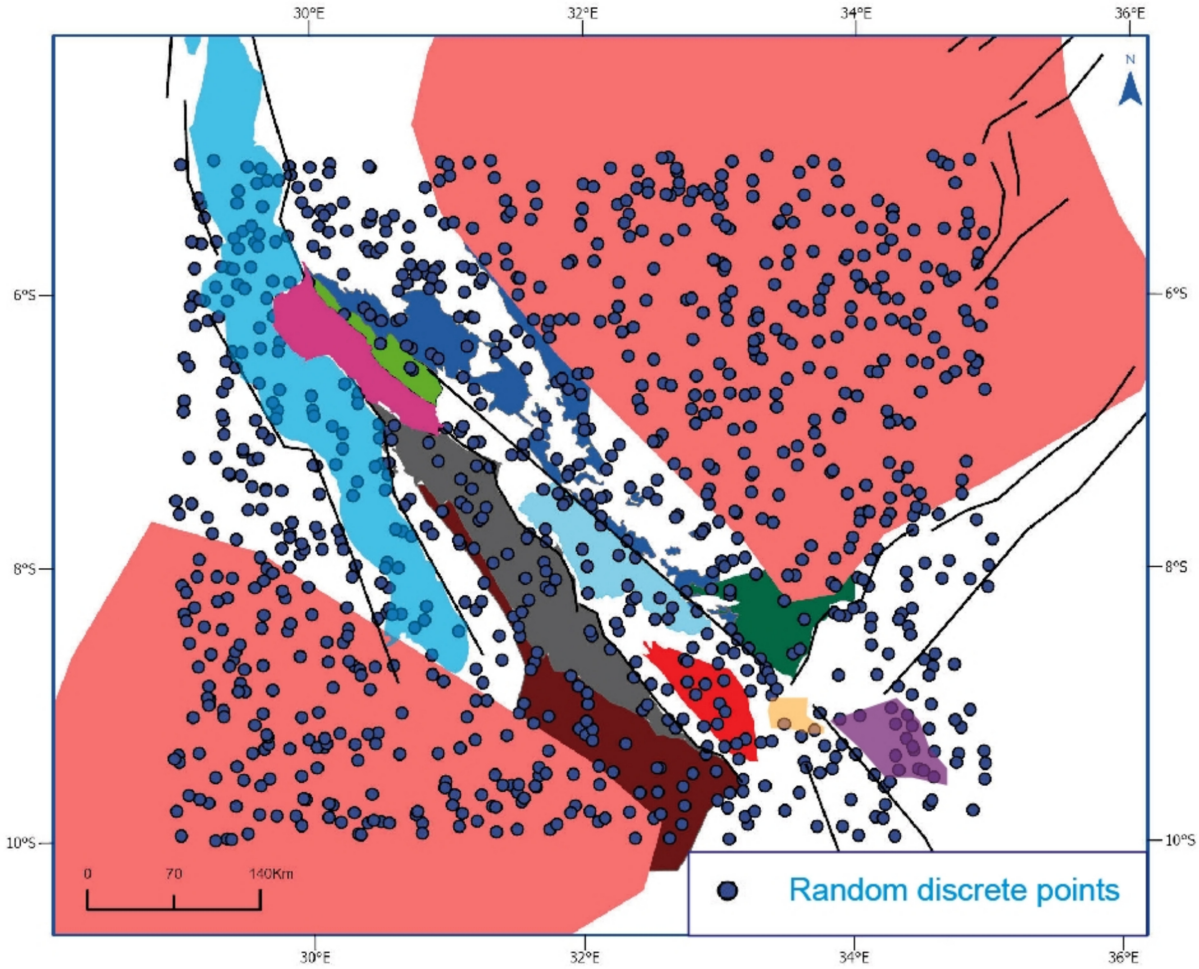

Fig. 2 Random discrete points (n = 1000) created on which heat flow, $CO_2/^3$He and ^{3}He/^{4}He data were interpolated over various tectonic terranes and averaged for use in mass computation and raster mapping (see Fig. 1 for legend)

m^2) (Fig. 3A, B). Our model reveals that the heat flow anomaly coincides with changes in topography with higher heat flow up to (99 mW/m^2) observed over the RVP highlands compared with the RRB graben with heat flow as low as ~64 mW/m^2 (Fig. 3A, B). Most of the high heat flow values are aligned with faults while others occur in accommodation zones (areas linking rift segments) and volcanically active area such as the RVP (Fig. 3A). The heat flow decreases significantly towards the distal areas from the RVP where the lowest heat flow up to ~32 mW/m^2 occurs in the Malawi Rift (Fig. 3A). Notably, further to the northeast of the Rukwa Rift, higher heat flow ~94 mW/m^2 is observed over the Lupa Terrane than any other tectonic terrane within the Ubendian mobile belt (Fig. 3A). The high heat flow over the Lupa Terrane is observed near the rift shoulder and horst blocks of both the Rukwa and Usangu rifts and decreases towards the distal areas (Fig. 3A).

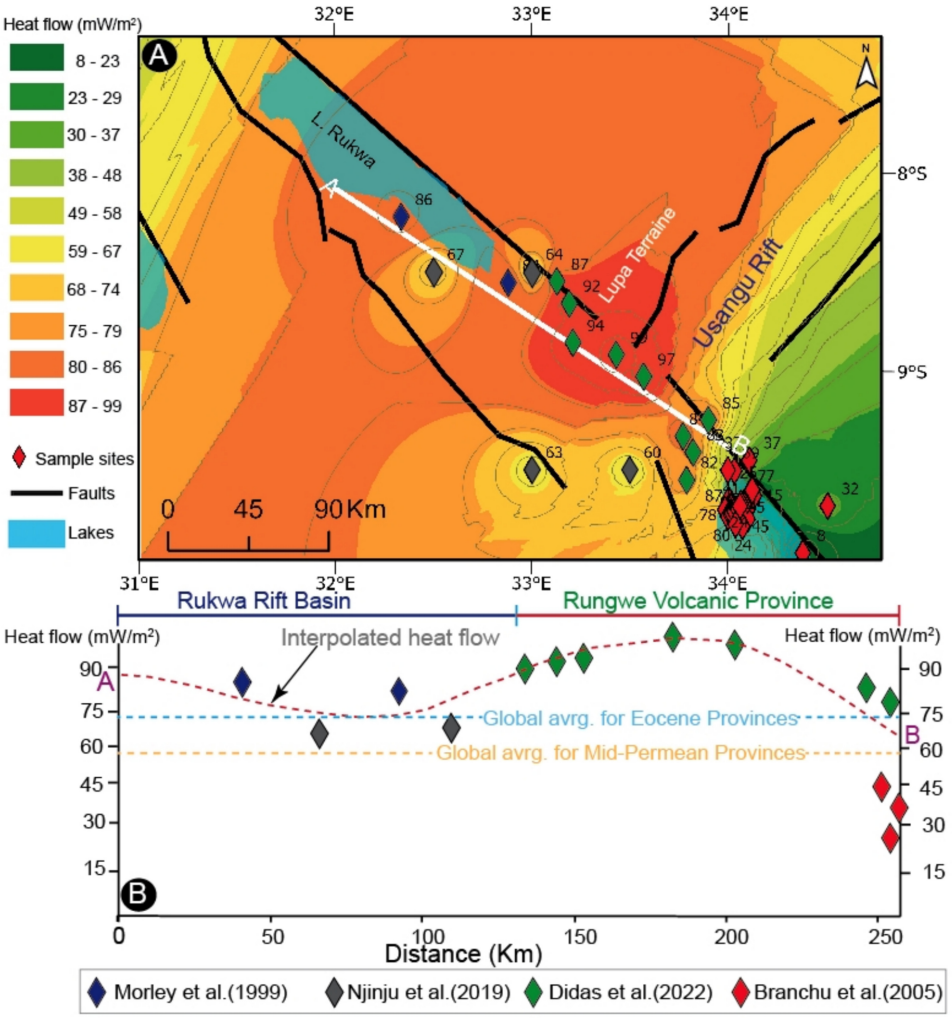

Fig. 3 (A) Map showing the distribution of heat flow between RRB and RVP generated from the statistical interpolation at various locations. (B) A profile showing distribution of heat flow values between the RRB and the RVP compared to the global mean heat flow for Mid-Permian and Eocene provinces (after Polyak and Smirnov 1968; Chapman and Pollack 1975; Njinju et al. 2019)

4.2 Relationship between heat flow and helium isotope ratio

The highest heat flow in the RVP (up to 99 mW/m^2) corresponds to the highest ^{3}He/^{4}He ratio (3.3–7.10 Ra) (Fig. 4A, B). In the RRB the lowest heat flow (64 mW/m^2) is associated with the lowest ^{3}He/^{4}He ratio (0.18–0.68 Ra) (Fig. 4A, B). The changes in a trend of helium isotopic ratio coincide with the changes in topographic profile (Fig. 4A–D).

4.3 Relationship between heat flow and $CO_2/^3$He ratio

The general trend of heat flow in relation to $CO_2/^3$He shows the highest heat flow (~99 mW/m^2) occurring in the RVP characterized by the highest $CO_2/^3$He (1.4×10^{13}–2.9×10^{13}) (Fig. 5A, B). The RRB reveals the lowest heat flow (~64 mW/m^2) corresponding to the lowest $CO_2/^3$He (0.5×10^{10}–1.0×10^{11}) (Fig. 5A, B). Similar to helium isotopic ratio, the change in $CO_2/^3$He along strike of the RRB and RVP show corresponding changes with topography (Fig. 5A-D; Fig. 6A–C).

4.4 Heat flow anomaly and frequent seismicity in the region

Our observation shows that seismicity swarms occur in areas of high heat flow (Fig. 7). Notably at the junction of border faults between the Rukwa Rift and Usangu Rift, frequent seismicity most likely revealing active tectonic activity and fault reactivation associated with thermal anomalies (Fig. 7).

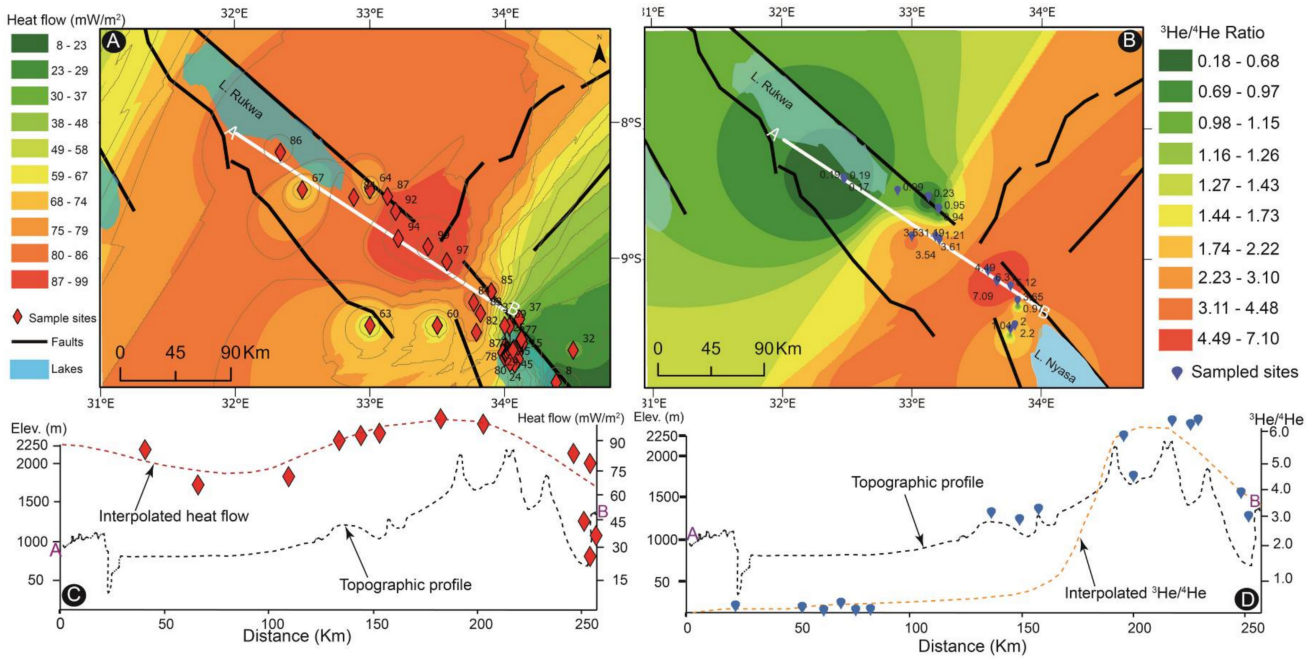

Fig. 4 (A) Interpolated heat flow map for the RVP and RRB. The diamond symbols show heat flow values that have been either tested or computed. (B) Raster map showing the distribution of $^{3}He/^{4}He$ ratios. Areas with available $^{3}He/^{4}He$ data are shown with blue drop symbols. (C) A profile across the southern part of the RRB and RVP showing distribution of interpolated heat flow against the topographic profile. (D) Section across the southern part of the RRB and RVP showing distribution of interpolated $^{3}He/^{4}He$ ratio against the topographic profile

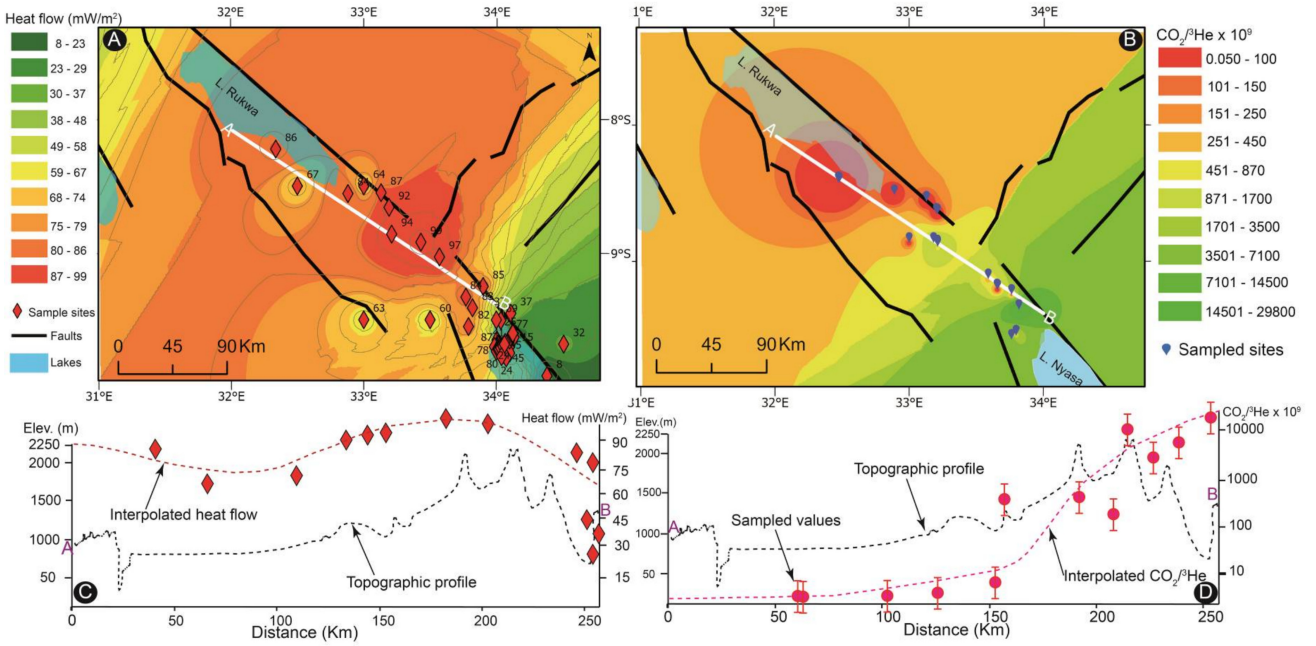

Fig. 5 **A** Interpolated heat flow map for the RVP and RRB. The diamond symbols show heat flow values where has been either tested or computed. **B** Raster map created from interpolation of available data to show the distribution of $CO_2/^{3}He$ ratios. Locations with available $CO_2/^{3}He$ data are shown with blue drop symbols. **C** A profile across the southern part of the RRB and RVP showing distribution of interpolated heat flow against the topographic profile. **D** A profile across the southern part of the RRB and RVP showing distribution of interpolated $CO_2/^{3}He$ ratio against the topographic profile

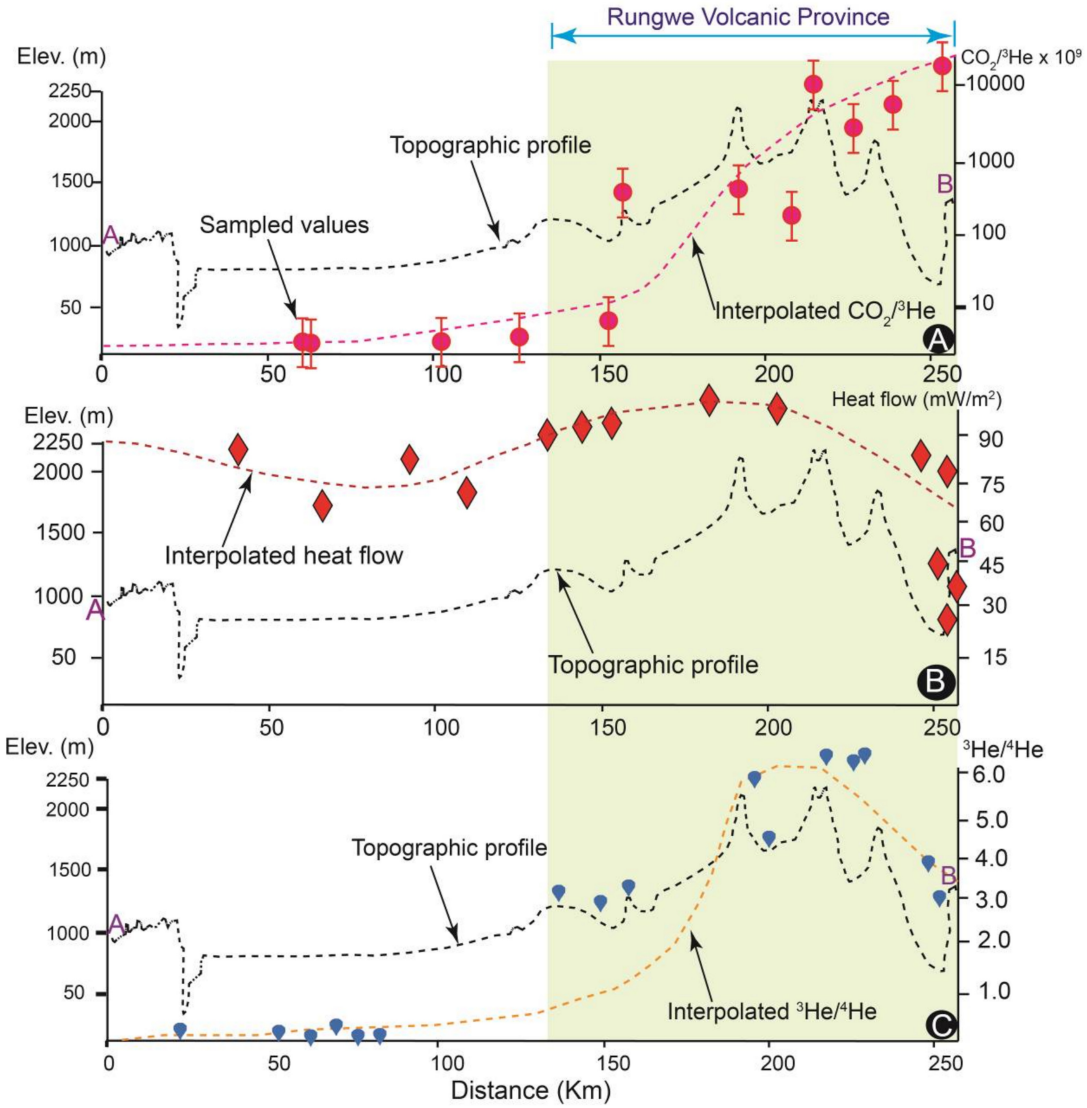

Fig. 6 Profile across the RVP and the southern part of the RRB showing distribution of **A** $CO_2/^3He$ ratio against the topographic profile. **B** heat flow against the topographic profile. **C** $^3He/^4He$ ratio against the topographic profile. (See Fig. 3A for location)

4.5 Helium potential of the East Africa Helium Pool (EAHP)

Helium isotopic ratios ($^3He/^4He$), expressed as Ra were interpolated as essential pre-computational values for use in mass balance calculation. The cratons with ~ 3 to 7 times the average crustal concentration of radioactive elements, have Ra distribution ranging between 1.3 Ra and 1.5 Ra (Tables 1, 2). The RRB presents the lowest Ra ~0.2 Ra in the system whereas, the Upangwa Terrane, Nyika Terrane and the RVP have the highest Ra ~3.3–3.7 Ra. The distribution of Ra in other terranes includes Ufipa ~1.1 Ra, Ubende ~1.2 Ra, Katuma ~1.2 Ra, Wakole ~1.2 Ra, Mbozi ~2.6 Ra, Lupa ~1.9 Ra and Kate Kipili ~1.6 Ra (Tables 1–2).

Mass balance computation for degassing and production of radiogenic helium show that the whole EAHP has a crustal mass of 7.0×10^{10} megatonnes which includes the Tanzania Craton, Bangweulu Craton and the Ubendian mobile belt (Table 3). The tectonic terranes and blocks surrounding the RRB are capable of producing at least 3.3×10^{-6} mol $^4He/m^2$ yr (Table 3). In addition, both the Bangweulu and the Tanzania cratons can potentially produce 6 times more than other terranes in the Ubendian mobile belt (~1.9×10^{-5} mol $^4He/m^2$ yr) making a total helium production rate of at least 2.2×10^{-5} mol $^4He/m^2$ yr in an area of ~614,000 km^2 for the Whole-Crust (1WC) under the assumption of a closed system EAHP (Table 3).

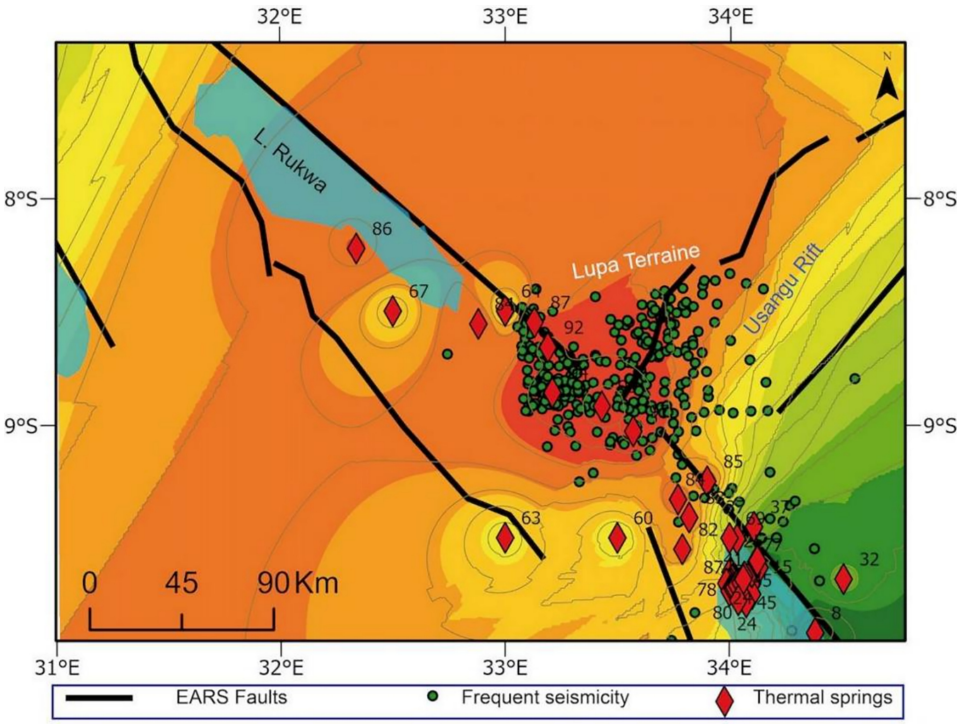

Fig. 7 Heat flow map overlain by the distribution of frequent seismicity recorded in the region. Note seismicity clusters occur at the junction between the Usangu Rift and Rukwa Rift

4.5.1 Helium degassing: case-I

Under this postulate we assume CO_2 flux of 4.05 tonnes/day over an areal extent ~981.5 km^2 (Lee et al. 2016; Table 1). Feasible models under this postulate suggest a total crustal ^{4}He emission of ~272WC from the EAHP (Table 1). The contribution of crustal ^{4}He emissions for each tectonic terrane include 124WC (46%) from the Tanzania Craton, 62WC (22%) from the Bangweulu Craton and 52WC (19%) from the crystalline basement of the RRB. The tectonic terranes in the whole Ubendian mobile belt constitute 36WC (13%) of the helium contribution in the region (EAHP) (Table 1).

Case-I shows total radiogenic helium flux ~2.68×10^9 mol/yr in the EAHP with areal extent ~614,000 km^2 (~4.4×10^{-3} mol ^{4}He/m^2 yr) (Table 1). Notably, in the RRB the calculated ^{4}He emissions reveal ~5.01×10^8 mol/yr in an area of ~8890 km^2 (~5.6×10^{-2} mol ^{4}He/m^2 yr) (Table 1). The ^{4}He emission in the RRB is thus equivalent to 19% of the total WC whereas in the RVP ~1500 km^2, the ^{4}He emissions are lower ~2.07×10^6 mol/yr (< 1%) than in the RRB (Table 1).

4.5.2 Helium degassing: case-II

This postulate assumes a CO_2 flux of 0.0055 tonnes/day over an areal extent ~1500 km^2 (Barry et al. 2013) which results in a crustal helium flux ~0.24WC (Table 2). Similar to Case-1 above, the Tanzania Craton contributes 46% of the crustal ^{4}He emission, Bangweulu Craton (21%), RVP (< 1%), the underlying crystalline basement of the RRB (21%) and the Ubendian mobile belt (12%).

Total radiogenic helium flux in the EAHP under Case II results in up to ~2.39×10^6 mol/yr (~3.9×10^{-6} mol ^{4}He/m^2 yr) (Table 2). Similar to Case-1, the calculated ^{4}He emissions under this case reveal ~4.45×10^5 mol/yr from an area of ~ 8890 km^2 of the RRB (~5.0×10^{-5} mol ^{4}He/m^2 yr). The radiogenic helium degassing in the RRB is thus equivalent to 21% of the WC. In the RVP, the helium emission is lower than in the RRB that is, ~1.84×10^3 mol/yr (~1.23×10^{-6} mol ^{4}He/m^2 yr) equivalent to < 1% (Table 2).

4.6 Radiogenic residence time in the Rukwa rift

Residence time are calculated using geochemical data which include resolved radiogenic isotopes ^{4}He and ^{40}Ar from uranium and thorium that were quantitatively recovered from fluids by Danabalan et al. (2022), Mtili et al. (2021) and Kimani et al. (2021). The calculations assume that these daughter isotopes were produced in situ and accumulated within the hydrological closed system of the Rukwa Rift which is comprised of the Rukwa Rift Basin and Rungwe Volcanic Province. Therefore, the residence time refers to the period since isolation of a daughter isotope and interaction with a hydrological system within either crystalline basement or overlying sedimentary units.

The radiogenic noble gas concentration of noble gas is calculated per volume of water using Gas–Water ratios (Vg/

Vw). The assumptions made for reference Air Saturated Water (ASW), initial pore fluid composition and salinity are adopted from Mtili et al. (2021). The ASW also assumes that the groundwater has undergone little or no changes that is, phase separation since last equilibration with the atmosphere (Holland et al. 2013; Warr et al. 2018). We further assume that all radiogenic noble gases were produced in situ either within sedimentary settings or from the deeper crust of the Rukwa Rift and accumulated in the stratigraphic sequences controlled dominantly by vertical diffusive migration (cf. Holland et al. 2013; Cheng et al. 2021). For instance, at Ivuna mudpots locality the average Vg/Vw of 0.0075 shown in Eq. (1);

$$\frac{V_g}{V_w}\left(36_{Ar}\right) = 0.0075 \tag{1}$$

This can be rewritten in Eq. (2) as;

$$\frac{V_g}{V_w}\left(36_{Ar}\right) = \frac{1}{133.3} \tag{2}$$

This means that at the Ivuna mudpots 1 cm^3 at Standard Temperature and Pressure (STP) of ^{36}Ar can be stripped out by 133.3 cm^3 of water in the subsurface. Since $^4He/^{20}Ne$ ratio in the Rukwa Rift ranges from 1–15,000 (Mtili et al. 2021), therefore the atmospheric contribution in the hydrologic closed system of the Rukwa Rift is either little or negligible.

Given the average concentrations of the $^{40}Ar/^{36}Ar$ ratio = 726 and $^{40}Ar = 16{,}175 \times 10^{-6}$ cm^3/cm^3 at Ivuna mudpots (Table 6).

The concentration of ^{36}Ar in equivalent volume of water is the concentration of $^{40}Ar \div {}^{40}Ar/^{36}Ar$ ratio, thus, $16{,}175 \times 10^{-6}$ cm^3 $/cm^3 \div 726 = 2.2\ 10^{-5} cm^3$ $/cm^3$ ^{36}Ar.

4.6.1 Noble gases accumulation in the hydrologic system of the Rukwa Rift: Case study of Ivuna mudpots

Since 1 cm^3 STP of ^{36}Ar can be stripped out by 133.3 cm^3 of water in the subsurface (Eq. 2), therefore groundwater ^{36}Ar concentration of $2.2 \times 10^{-5} cm^3$ $/cm^3$ will require 2.97×10^{-3} cm^3 of subsurface water that is, the total volume of water that the noble gases have interacted with beneath the Ivuna mudpots. This amount of water can therefore be used to compute the concentration of other radiogenic noble gases per equivalent volume of water sampled from the same locality.

Using the equivalent volume of water as 2.97×10^{-3} cm^3, the concentration of $^{40}Ar = 16{,}175 \times 10^{-6}$ cm^3/cm^3 per volume of water will be 5.45 cm^3/cm^3 H_20. Similar algorithms can be applied for the resolved ^4He concentration.

In order to calculate the noble gas concentration, the reasonable estimate of the rock matrix density and measured porosity were considered based on assumptions made also by Warr et al. 2018 (Eq. 3);

$$\begin{aligned}\text{Conc.}40_{\text{Ar}}\left[\frac{\text{cm3}}{\text{gram}}\text{of host rock}\right] \\ = 40_{\text{Ar}}\left[\frac{\text{cm3}}{\text{cm3}}\text{of water}\right] \times \text{Porosity} \div \text{Density}\end{aligned} \tag{3}$$

where density = 2.7 g/cc and porosity measurements are 11.8% for the Lake Beds Group, 30% for the Red Sandstone Group, 26% Karoo Supergroup and Precambrian Basement is 0.64% (Chaki et al. 2008).

Substituting Eq. (3) into the radiogenic dating Eq. (4) described by Warr et al. 2018 and references therein.

$$\text{Conc.}40_{\text{Ar}}\left[\frac{\text{cm}^3}{\text{gram}}\text{ of host rock}\right] = 0.105 \times 40_{\text{K}} \times \left[e^{\lambda_{40} t} - 1\right] \tag{4}$$

Solving for residence time 't' for K–Ar equation will lead to Eq. (5);

$$\text{t} = \frac{\ln\left[\frac{40_{\text{Ar}} + (0.105 \times 40_{\text{Ar}}}{0.105 \times (40_{\text{K}})}\right]}{\lambda_{40}} \tag{5}$$

Similarly solving for radiogenic residence time 't' for U-Th/He Eq. (6) will lead to a solution shown in Eq. (7);

$$\begin{aligned}4_{\text{He}} = 8 \times (238_{\text{U}}) \times \left[\text{e}^{\lambda_{238}\text{t}} - 1\right]) + 7 \times (235_{\text{U}}) \times \left[\text{e}^{\lambda_{235}\text{t}} - 1\right] \\ + 6 \times (232_{\text{Th}}) \times \left[\text{e}^{\lambda_{232}\text{t}} - 1\right]\end{aligned} \tag{6}$$

$$t = \left[\frac{\frac{\ln[(4_{He}) \times 8 \times (238_U) \times 7 \times (235_U) \times 6 \times (232_{Th})]}{\ln\left[8 \times (238_U) \times 7 \times (235_U) \times 6 \times (232_{Th})\right]}}{\lambda_{238} + \lambda_{235} + \lambda_{232}}\right] \tag{7}$$

where ^{238}U, ^{235}U, ^{232}Th and ^{40} K are elemental concentrations in the host rock including; U-238 (2.8 ppm), U-235 (2.8 ppm), U-232 (10.7 ppm) (Manya et al. 2007; Mshiu and Maboko 2012) and K-40 (2%) (Warr et al. 2018) respectively. The decay constants per year with values in parenthesis are as λ_{238} (0.155125×10^{-9} yr^{-1}), λ_{235} ($0.98485 \times 10–^{9}$ yr^{-1}), λ_{232} (0.049475×10^{-9} yr^{-1}) (Davis and Villeneuve 2001; Parsons-Davis et al. 2018; Brevart et al. 1982 and references therein) and λ_{40} (0.557×10^{-10} yr^{-1}) (Wetherill et al. 1956). The results for these radiogenic ages are as shown in Tables 6 & 7).

5 Discussion

5.1 Crustal radiogenic helium 'kitchen'

Our models reveal that the entire rock volume of the Tanzania Craton contributes to 46% – 50% (∽124WC) of ^4He flux in the EAHP (Table 1). The estimated average helium production potential in the whole EAHP sums to ~ 22×10^{-6} mol

$^4He/m^2$ yr including the cratons ~ 19×10^{-6} mol $^4He/m^2$ yr and the Ubendian mobile belt ~ 3.3×10^{-6} mol $^4He/m^2$ yr (Tables 1 and 2). These values are generally greater (up to ~ 9 times) than the global statistical averages calculated for major sedimentary basins which are up to ~ 1.74×10^{-6}—2.2×10^{-6}—mol $^4He/m^2$ yr (Torgersen 2010; Cheng et al. 2021). Elsewhere previous studies have reported helium flux from continental crust settings such as the Paris Basin ~ 0.2×10^{-6}–7.9×10^{-6} mol $^4He/m^2$ yr and the Great Artesian Basin ~ 0.9×10^{-6}–1.6×10^{-6} mol $^4He/m^2$ yr, Saskatchewan lakes ~ 0.2×10^{-6}–52×10^{-6} mol $^4He/m^2$ yr and Williston Basin ~ 0.29×10^{-6}-1.34×10^{-6} mol $^4He/m^2$ yr which are inline with this study (Torgersen 2010; Cheng et al. 2021).

Such a significant amount of ^4He flux in the EAHP would require massive impingement of high heat flow triggering helium release most likely related to a mantle plume beneath the Tanzania Craton (Pik et al. 2006; Ebinger and Sleep 1998; Danabalan et al. 2022). For the Tanzania Craton, a thermal surge has been previously evidenced from thermal springs, seismic tomography and diamond kimberlitic rocks which serve as unique proxy for metasomatism and heat flow aspects in the region (e.g.Bulanova et al. 2004; Stiefenhofer and Farrow 2004; Park and Nyblade 2006; Brown et al. 2012; Ebinger et al. 2013). Since the Tanzania Craton has the highest contribution to ^4He flux (124 WC), it is likely that cratonic foundering and metasomatic weakening facilitates ^4He release and circulation over large distances throughout the region (e.g.Shirey et al. 2013; Danabalan 2017; Table 1). Due to the fact that the crustal thickness in the region varies (Kachingwe et al. 2015; Didas et al. 2022), it is possible that the asymmetric geometry of a cratonic 'keel' associated with lithospheric-scale faults, may deflect the mantle plume unevenly between the two branches of East Africa Rift System (Koptev et al. 2015; Fig. 8). Similar to suggestions by Koptev et al. (2015), the variation of isotopic ratios and heat flow observed in this study over the RRB and the RVP may also support the asymmetrical magmatic and non-magmatic nature of the East African Rift System.

Since the helium production is a continuous process, several degassing models in this study (e.g., Tables 4 and 5) could suggest that the ^4He mass balance is largely affected by degassing surges triggered by transient tectonothermal regimes. However, since the heat flow decay in the continental crust takes up to ∽~800 Myrs (e.g. Sclater et al.1980; Hu et al. 2000), each successive tectonothermal event recorded in the Rukwa Rift (Mulaya et al. 2022), implies transient degassing surges followed by a hiatus of crustal stability and tectonic quiescence associated with normal degassing under a steady-state thermal regime. We postulate that heat transfer from the plume magmatism makes a significant contribution to the conductive and convective heat flow recharge, injection and fluid dynamics in the region (e.g., Lysak 1992; Ebinger and Sleep 1998; Pik et al. 2006; Fig. 8). Notably high heat flow up to 99 mW/m^2 for the Rungwe Volcanic Province reflects a local thermal anomaly associated with

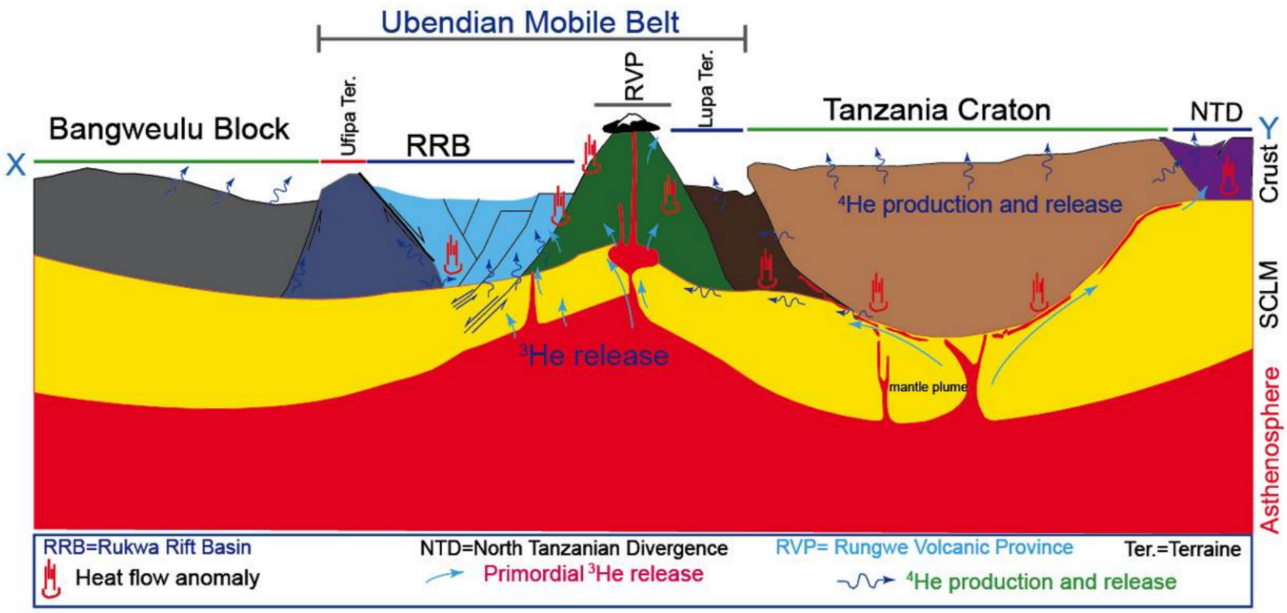

Fig. 8 Conceptual model showing the heat flow distribution for the EAHP related to plume magmatism. The heat flow anomaly triggered by the tectonothermal event is essential for releasing radiogenic helium from the continental crust. NTD. North Tanzanian Divergence; RRB. Rukwa Rift Basin; RVP. Rungwe Volcanic Province; SCLM. Sub-Continental Lithospheric Mantle (SCLM) (refer to Fig. 1A for map location) (after Koptev et al. 2015; Mtili et al. 2021; Kimani et al. 2021; Danabalan et al. 2022)

Table 4 Average radiogenic ages for each sampling locality based on the ^{40} K-^{40}Ar Equation relating radiogenic isotopes where average residence times are calculated using bulk porosity (**Φ**) of each lithostratigraphic units in the Rukwa Rift Basin which are Lake Beds Group (LKB), Red Sandstone Group (RSS), Karoo and Basement. Concentrations of ^{40}Ar isotopes expressed per cm^3 of pore water (degassed water volume) of respective lithology using Vg/Vw after Mtili et al. (2021), Warr et al. (2018), Holland et al. (2013). For each level both individual samples and an average concentration is presented

Sample Location	[Vg/Vw] ^{36}Ar	^{40} Ar [cm^3 STP/cm^3]	^{40}Ar [cm^3/ cm^3 H_2O]	Φ [LKB]	Φ [RSS]	Φ [Karoo]	Φ [Basement]	Density [g/cc]	^{40} K ppm	λ_{40} Yr-1	Ages [LKB]	Ages [RSS]	Ages [Karoo]	Ages [Basement]
Ivuna mud-pots	7.50E-03	1.62E−02	5.45	0.118	0.3	0.26	0.0064	2.7	2.00E+04	5.57E−11	2.0E+06	5.17E+06	4.48E+06	1.10E+05
Itumbula salt pond	4.83E-02	9.59E−03	38.40	0.118	0.3	0.26	0.0064	2.7	2.00E+04	5.57E−11	1.4E+07	3.64E+07	3.16E+07	7.78E+05
Kajundu spring	4.40E-02	3.99E−03	13.90	0.118	0.3	0.26	0.0064	2.7	2.00E+04	5.57E−11	5.2E+06	1.32E+07	1.14E+07	2.81E+05
Tete spring	6.20E-02	3.10E−03	18.50	0.118	0.3	0.26	0.0064	2.7	2.00E+04	5.57E−11	6.9E+06	1.75E+07	1.52E+07	3.75E+05
Ibaya spring	4.32E+00	8.13E−05	1450.00	0.118	0.3	0.26	0.0064	2.7	2.00E+04	5.57E−11	5.3E+08	1.32E+09	1.15E+09	2.93E+07
Ngwilo spring	2.61E-01	1.37E−03	94.40	0.118	0.3	0.26	0.0064	2.7	2.00E+04	5.57E−11	3.5E+07	8.95E+07	7.76E+07	1.91E+06
Nanyara spring	3.88E+00	7.35E−05	1400.00	0.118	0.3	0.26	0.0064	2.7	2.00E+04	5.57E−11	5.2E+08	1.28E+09	1.12E+09	2.83E+07
Songwe river	2.05E+01	1.69E−05	6420.00	0.118	0.3	0.26	0.0064	2.7	2.00E+04	5.57E−11	2.3E+09	5.25E+09	4.63E+09	1.30E+08

Table 5 Average radiogenic ages for each sampling locality based on equation relating radiogenic uranium, thorium and helium isotopes. The average residence times are calculated using bulk porosity (**Φ**) of each lithostratigraphic units in the Rukwa Rift Basin which are Lake Beds Group (LKB), Red Sandstone Group (RSS), Karoo and Basement. Generally, the age ranges in Neo-Mesoproterozoic period (See description in text)

Sample Location	^{4}He [cm^{3}STP/cm^3]	^{4}He [cm^3/cm^{3}H$_2$O]	^{4}He [cm^3/gm Rock]	[Vg/Vw] ^{36}Ar	^{238}U[ppm]	^{232}Th [ppm]	λ_{238} Yr^{-1}	$\lambda_{235\ Yr\text{-}1}$	$\lambda_{232\ Yr}{}^{-1}$	Ages [LKB]	Ages [RSS]	Ages [Karoo]	Ages [Basement]
Ivuna mud-pots	4.7E−02	1.58E+01	6.9E−01	0.0075	2.8	10.7	1.55E−10	9.85E−10	4.95E−11	8.1E+08	8.9E+08	8.8E+08	5.7E+08
Itumbula salt pond	3.4E−02	1.36E+02	6.0E+00	0.04825	2.8	10.7	1.55E−10	9.85E−10	4.95E−11	9.9E+08	1.1E+09	1.1E+09	7.5E+08
Kajundu spring	2.0E−04	6.95E-01	3.0E−02	0.044	2.8	10.7	1.55E−10	9.85E−10	4.95E−11	5.5E+08	6.3E+08	6.2E+08	3.1E+08
Tete spring	8.0E−03	4.77E+01	2.1E+00	0.062	2.8	10.7	1.55E−10	9.85E−10	4.95E−11	9.0E+08	9.8E+08	9.7E+08	6.6E+08
Ibaya spring	1.0E−04	1.78E+03	7.8E+01	4.32	2.8	10.7	1.55E−10	9.85E−10	4.95E−11	1.2E+09	1.3E+09	1.3E+09	9.6E+08
Ngwilo spring	1.1E−03	7.23E+01	3.2E+00	0.2605	2.8	10.7	1.55E−10	9.85E−10	4.95E−11	9.4E+08	1.0E+09	1.0E+09	7.0E+08
Nanyara spring	2.0E−05	3.76E+02	1.6E+01	3.8825	2.8	10.7	1.55E−10	9.85E−10	4.95E−11	1.1E+09	1.1E+09	1.1E+09	8.3E+08
Songwe river	7.8E−07	2.97E+02	1.3E+01	20.4935	2.8	10.7	1.55E−10	9.85E−10	4.95E−11	1.1E+09	1.1E+09	1.1E+09	8.1E+08

tectonics and suggests a possible mechanism for continual heat flow recharge in the EAHP (e.g., Njinju et al. 2019; Fig. 8). However, a tectonothermal event related to a mantle plume may not necessarily be the only thermal source as radiogenic heat production and intra-crustal magma chambers may contribute to the heat surge in the region (Sclater et al. 1980; Pollack 1982). The assumption made for degassing and migration of crustal ^{4}He may equally depend on other factors in place such as the intensity of crustal opening such as fracturing, efficiency of release from the helium bearing minerals and concentration of other carrier fluids (Halford et al. 2022; Danabalan et al. 2022).

5.2 Implication of heat flow anomalies for helium potential

The occurrence of heat flow anomalies in the Rukwa Rift marked by corresponding changes in the topographic profile coincides with notable changes in isotopic ratios (Figs. 4D, 6B). This relationship can be observed on a profile across the RRB and the RVP where the changes in isotopic ratios $CO_2/^3$He and ^{3}He/^{4}He coincide with changes in topography (Fig. 6A–C). The relationship of heat flow to ^{3}He/^{4}He and $CO_2/^3$He is attributable to binary mixing trend between crust-derived gases and magmatic-derived gases whereas proximity to active volcanic center that is, RVP accounts for CO_2 anomaly (Mtili et al. 2021; Danabalan et al. 2022).

Pronounced high topography over the RVP up to ~2250 m is associated with anomalously high heat flow (~99 mW/m^2) and isotopic ratios that is, high $CO_2/^3$He ~1.4×10^{13}–2.9×10^{13} and high ^{3}He/^{4}He ~3.3–7.0 (Fig. 6A-C). The topographic high in the RVP may be related to crustal uplift due to a thermo-kinematic anomaly contributing to regional stress fields reflecting extension tectonics and doming in the region (Mareschal and Gliko 1991; Negredo et al. 1995).

The anomalies of heat flow and isotopic ratio in some places coincide with tectonically active fault networks in the RRB and RVP most likely due to increased porosity and deep-rooted fracture/fault permeability (Lysak 1992; Mulaya et al. 2022; Halford et al. 2022; Fig. 8). The evidence of the heat flow anomaly occurring along/proximal to faults and accommodation zones in the Rukwa Rift reveal tectonic strain and permeable conduit systems which may facilitate fluid migration in the region (e.g., Lowenstern et al. 2014; Halford et al. 2022; Mulaya et al. 2022). The fact that the seismicity record and geodetic studies show high frequency of earthquakes with significant magnitude (e.g., Stamps et al. 2018; Fig. 7) implies heat flow anomaly is associated with active tectonics which could influence fluid migration. Thermal anomalies in active tectonics have been associated with circulation of hydrothermal fluid and seismicity in the region (e.g., Wilks et al. 2017).

Table 6 **Postulate**-I: Helium emissions and accumulation models for various tectonothermal events in the Rukwa Rift Basin. *Note* the models highlighted in green show realistic cases

CASE - I	Accumulation Time (Myr)	Initial Production (at least)
MODEL - I: Assuming similar 4He emissions were discharged since onset of East African rifting coeval with magmatism (8.6 Ma- Harkin 1960; Ebinger 1989) via the whole region	2.34E+03	2349 Palaeoproterozoic
MODEL - II: Assuming similar 4He emissions were discharged during the onset of East African rifting coeval with magmatism (8.6 Ma- Harkin 1960; Ebinger 1989) via only Rukwa Basin and RVP	4.E+02	409 Ma (Early Devonian)
MODEL - III: Assuming similar 4He emissions were discharged since onset of Karoo rifting via the whole region (Late Carboniferous 300 Ma-Delvaux 2001)	8.16E+04	
MODEL - IV: Assuming similar 4He emissions were discharged since onset of Karoo rifting via the Rukwa Rift (Late Carboniferous 300 Ma-Delvaux 2001)	1.52E+04	
MODEL - V: Assuming similar emissions were discharged since Cretaceous Carbonatite magmatism (120 Ma) via whole region	3.26E+04	
MODEL - VI: Assuming g similar emissions were discharged since Cretaceous Carbonatite magmatism (120 Ma) via Rukwa Rift	6.E+03	

More than 50% of the $CO_2/^3He$ ratios in this study range between ~0.5×10^{10} and 2.9×10^{13} (Figs. 5A, B and 6A) that implies a binary source between crust and mantle signatures in the Rukwa Rift as suggested by Barry et al. (2013) and Danabalan. (2017). The observed spatial variation of geochemical anomalies and heat flow along the strike of the Rukwa Rift segments may be attributable to a bimodal crustal thickness distribution ~29 and 42 km previously reported in the region (e.g., Last et al. 1997; Plasman et al. 2017; Borrego et al. 2018). This lithospheric thickening and thinning profile may have caused a variable rifting intensity and fluid dynamics (e.g., Lysak 1992; Lemna et al. 2019; Kolawole et al. 2021; Kimani et al. 2021; Mtili et al. 2021; Mulaya et al. 2022). Similarly, the variation of active strain patterns mostly inherited from Karoo fabrics may equally modulate the heat flow through deflection of thermal weakening effects within individual rifts (Bellahsen et al. 2013; Kolawole et al. 2021; Mulaya et al. 2022).

Along the East Africa Rift System, heat flow has been reported to vary considerably depending on the stages of rifting with highest heat flow recorded in the Afar Rift (~150–250 mW/m^2) while the lowest is in the Malawi Rift ~8–24 mW/m^2 (Lysak 1992; Jones 2020; Fig. 3a). However, the heat flow values in the RRB and RVP are higher than both the average value for continental provinces ~49 mW/m^2 (Sclater 1980) and the global average for Mid-Permian provinces (~58 mW/m^2) during deposition of Karoo sediments (Polyak and Smirnov 1968; Chapman and Pollack 1975; Kilembe and Rosendahl 1992; Njinju et al. 2019; Fig. 3B). Most of the heat flow data values are also above the global average for recent Eocene Provinces ~72 mW/m^2 and differs by 10%–18% (Polyak and Smirnov 1968; Chapman and Pollack 1975; Fig. 3A, B).

5.3 Reconstructing helium accumulation models

A number of feasible closed system models for various terranes surrounding the RRB provide insights into the mass balance between helium production and flux in the EAHP. These models are considered under two major postulates (Postulate 1 & 2) which correspond to the two cases of helium flux model (Case I & II) through specific area/terrane of conduits. Each postulate reveals fluid dynamics during certain tectonothermal events which acted as a 'catalyst' for helium production andrelease surge by assuming 100% efficiency of helium release in the region. The tectonothermal events which have been previously mapped include; initiation of the Karoo rifting (~300) (Kilembe and Rosendahl 1992; Delvaux 2001); carbonatite volcanism (~120 Ma) (Boniface 2017) and the recent East African rifting coeval with magmatism (8.6 Ma); (Ebinger et al. 1989; Ebinger and Sleep 1998).

5.3.1 Postulate—1

We illustrate six helium accumulation and degassing models based on helium degassing Case-I and in relation to tectonothermal events recorded in the RRB (e.g., Danabalan et al. 2022; Mulaya et al. 2022). Although six models were considered (Table 1), only two models can explain feasibly the volume of ^4He emissions from the EAHP;

(1) *MODEL-I* Assuming constant ^4He emissions were discharged since the onset of East African rifting coeval with magmatism to date (8.6 MaHarkin 1960; Ebinger et al. 1989) via the whole region (EAHP) (Table 6; Fig. 9a). This model shows unmatched mass balance between helium production and helium flux. In order to account for this unbalanced scenario, the

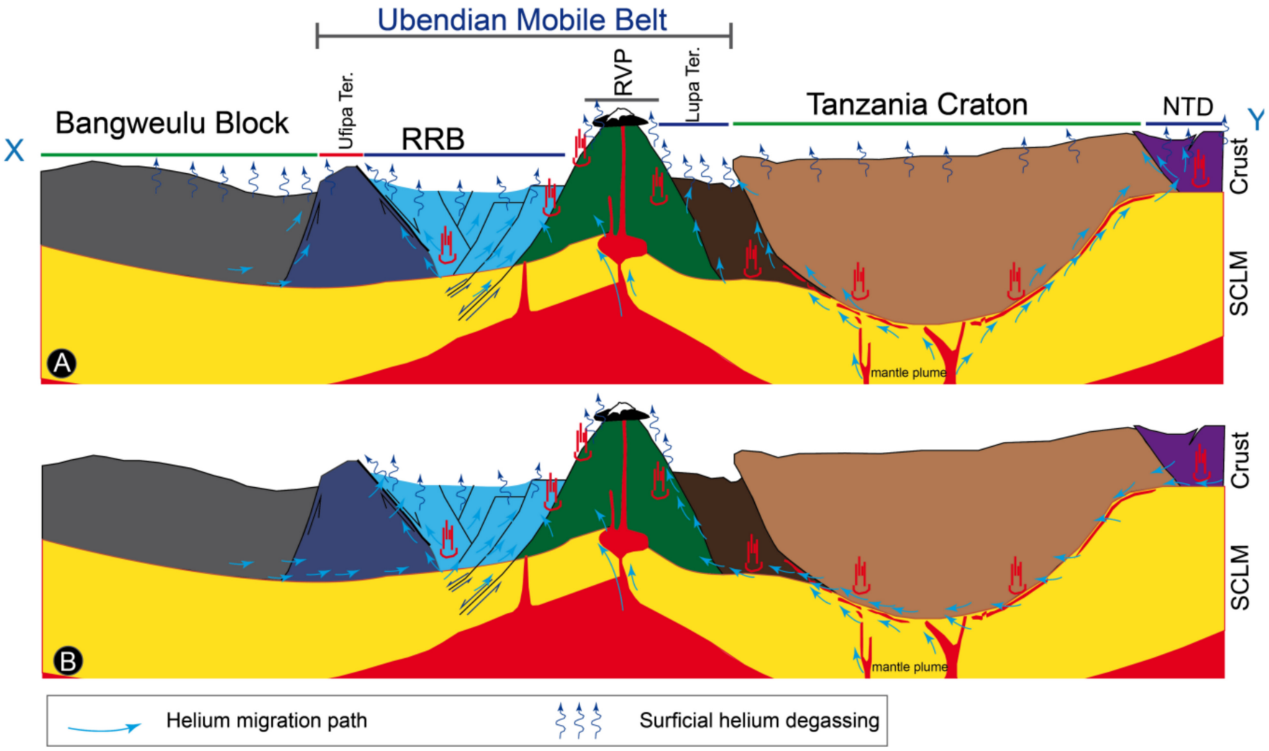

Fig. 9 Conceptual model showing the current helium migration and degassing model for the whole East Africa Helium Pool. **A** radiogenic degassing via the whole EAHP region. **B** degassing via the Rukwa Rift Basin (RRB) and the Rungwe Volcanic Province (RVP). Note the arrowhead indicates a proposed direction of regional migration

whole rock volume under the EAHP must have started ^{4}He production since at least the Palaeoproterozoic (2.349 Ga) with residence/accumulation time of at least 2340 Ma (Table 6). This timing coincides with the previously reported last phase of metamorphism in the Tanzania Craton at 2.4 Ga which serves as a proxy for high heat flow in the region (Pinna et al. 1994; Weeraratne et al. 2003; Danabalan et al. 2022).

MODEL—II Assuming ^{4}He emissions similar to those we observe today were discharged during the onset of East African rifting coeval with magmatism (8.6 Ma, Harkin 1960; Ebinger et al. 1989) via the Rukwa Basin and RVP which serve as the main conduits only. This degassing model can only be explained if the ^{4}He production had started since the Early Devonian (409 Ma) and accumulated for at least 400 Ma (Table 6; Fig. 9b).

Under Postulate-1, the mass balance calculations show that four models (Model-III-VI) out of six do not provide reasonable values since the degassing yields more radiogenic helium (hundred to thousand times) than the production capacity of the underlying crust. The assumption of a closed system model does not apply here since the accumulation time would extend far beyond the age of the Earth (beyond 4.6 Ga). Therefore, the unbalanced mass computation between ^{4}He flux and production for these models may otherwise imply an open system involving an exogenous source rather than a closed a system within the EAHP only (e.g., Halford et al. 2022).

5.3.2 Postulate—2

Mass balance results based on the assumption of the helium degassing model for Case II illustrated above and six plausible models for the helium production and release. These models assume 100% for both production and release efficiency from the source rocks within the EAHP.

(1) *MODEL-I* Assuming ^{4}He emissions similar to those we observe today were discharged during the onset of East Africa rifting and coeval with magmatism (8.6 Ma, Harkin 1960; Ebinger et al. 1989) via the whole region (EAHP). This model suggests that the production capacity of the EAHP crustal rock volume would take 2.08 Myr to accumulate crustal ^{4}He in the region. The helium production would have therefore started in the Miocene (10.8 Ma) to account for the current flux rate observed in the region (Barry et al. 2013; Lee et al. 2016; Table 7; Fig. 9A).

Table 7 Postulate 2: Helium emissions and accumulation models for various tectonothermal events in the Rukwa Rift Basin

CASE–II	Accumulation time (Myr)	Initial production (at least)
MODEL–I Assuming similar 4He emissions were discharged during onset of East African rifting coeval with magmatism (8.6 Ma, Harkin 1960; Ebinger et al. 1989) via the whole region	2.08E + 00	10.68 Ma (Miocene)
MODEL–II Assuming similar ^{4}He emissions were discharged since onset of East African rifting coeval with magmatism (8.6 Ma, Harkin 1960; Ebinger et al. 1989) via only Rukwa Basin and RVP	3.89E−01	389 Ka (Quaternary)
MODEL–III Assuming similar 4He emissions were discharged since onset of Karoo rifting via the whole region (Late Carboniferous 300 Ma, Delvaux 2001)	7.25E + 01	372.5 Ma (Late Devonian)
MODEL–IV Assuming similar ^{4}He emissions were discharged since onset of Karoo rifting via the Rukwa Rift (Late Carboniferous 300 Ma, Delvaux 2001)	1.36E + 01	313.6 Ma (Pennsylvanian)
MODEL–V Assuming similar emissions were discharged since Cretaceous Carbonatite magmatism (120 Ma) via whole region	2.90E + 01	149 Ma (Late Jurassic)
MODEL–VI Assuming similar emissions were discharged since Cretaceous Carbonatite magmatism (120 Ma) via Rukwa Rift conduits	5.43E + 00	125.43 Ma (Early Cretaceous)

(2) *MODEL-II* This model is similar to Model-I above except that we assume the conduits of fluid flow to include both the Rukwa Basin and the RVP. The combined conduit areas over ^{4}He emission would therefore be smaller than the volume of rock and helium production capacity in the EAHP. The accumulation minimum time would therefore be reduced to helium released recently since the Quaternary (389 Ka) (Table 7; Fig. 9b).

(3) *MODEL-III* In this model we postulate that the tectonothermal event during Karoo rifting from late Carboniferous 300 Ma (Delvaux 2001) would have paved a way for crustal instability and break up associated with helium release in the region. We therefore assume similar ^{4}He emissions observed today were discharged since onset of Karoo rifting where the helium was vented off through the whole region (EAHP). This model suggests that production of helium must have been started since the Late Devonian (372.5 Ma) having potentially accumulated for at least 72.5 Ma (Table 7).

(4) *MODEL-IV* This model is similar to Model-III except the ^{4}He was vented through the Rukwa Rift only. To account for this emission, the helium production would have started since the Pennsylvanian time (313.6 Ma) and accumulated for 13.6 Ma (Table 7).

(5) *MODEL-V* Assuming similar emissions we observe today were discharged since the Cretaceous (120 Ma) during carbonatite magmatism via the whole region (EAHP). Under this model, helium production would have initiated during the Late Jurassic (149 Ma) for the residence period of at least 29 Ma (Table 7).

(6) *MODEL-VI* We assume similar conditions to Model-V except that the conduits for ^{4}He emissions were discharged via the Rukwa Rift. The time for helium release and accumulation would be 5.43 Ma which started during the Early Cretaceous (125.43 Ma). This timing coincides with the previously reported carbonatite volcanism in the Rukwa Rift hence implying the influence of heat flow surge associated with rifting associated with volcanic diking events hence contributing to helium release. During this time the Red Sandstone sequences were simultaneously depositing whereas the Karoo sequences had already deposited with Top Karoo unconformity in place (Mulaya et al. 2022). Therefore, this timing could have favored accumulation of radiogenic helium in the Karoo sedimentary sequences. The petrophysical analysis of the Karoo sequences has been analyzed previously as 660.6 mD permeability and 26% porosity hence making it potential reservoir for helium accumulation.

The estimate of radiogenic ages for noble gases sampled in the Rukwa Rift show a bimodal cluster of noble gas release surges during recent East Africa Rift System and Pan-African orogenic cycles respectively (Fig. 10). The two episodes are known to have been associated with magmatism and metamorphism respectively (Ebinger et al. 1989; Boniface 2009). We infer that although helium has been continually generated from basement since the Precambrian to date, the release surges were during the Pan-African orogenic cycles and the recent East Africa Rift System. The mechanism of migration of released radiogenic noble gases most likely involved mainly vertical diffusion followed by petrophysical entrapment in pore fluids of the lithostratigraphic sequences in the Rukwa Rift (e.g., Cheng et al. 2021). However, for both K–Ar and U-Th/He methods, some of the computed ages from the same locality show a disparity in the radiogenic ages. Age disparity between calculated and known ages of lithostratigraphic units most likely imply an exogenous source for radiogenic noble gases via vertical

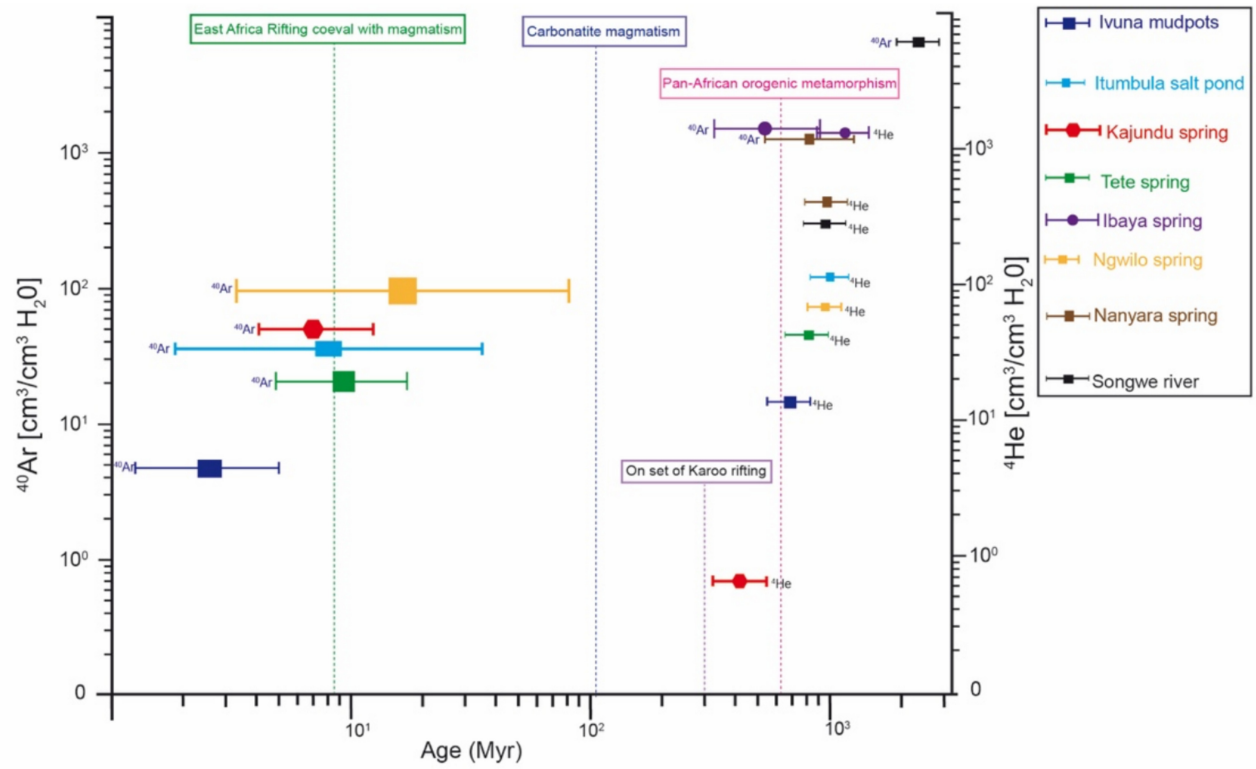

Fig. 10 Distribution of average radiogenic ages given in Ma based on ^{40}Ar and ^{4}He for eight ($N=8$) sampling locality in the Rukwa Rift (adopted from Warr et al. 2018). The observed uncertainty in ages is due to variation of porosities as discrete inputs in calculation of radiogenic ages which include 11.8% (Lake Beds Group), 30% (Red Sandstone Group), 26% (Karoo Supergroup) and 0.64% (Precambrian Basement) based on petrophysical analysis (Chaki et al. 2008). Note the two clusters of radiogenic helium release during the Precambrian Pan-African orogenic cycles and the recent East Africa Rift System. Major regional geological events are based previous publications (Ebinger et al. 1989; Kilembe and Rosendahl 1992; Delvaux 2001; Boniface 2009)

diffusion of helium within a closed system that is, overlying sedimentary units supplied by Precambrian Basement (e.g., Cheng et al. 2021). Disparities of radiogenic ages may also imply interplay of other factors e.g. assumptions made in each method and history path of radiogenic minerals including, slow cooling of rocks, alteration and recrystallization of clock minerals which can not be ruled out in this study (e.g., Curtis and Reynolds. 1958; Lippolt et al. 1994; Taylor and Aitken. 1997).

6 Conclusions

Mass balance computation in this study concludes that a comprehensive closed system of the EAHP has a crustal mass of ~7.0×10^{10} megatonnes and has the capability of producing ^{4}He of about ~9.9×10^{6} mol per year. The Tanzania Craton contributes largely to radiogenic helium production and release contributing up to 50% in the region. Such helium accumulation in the EAHP would have started since the Paleoproterozoic. However, subsequent release has been accelerated largely by episodic tectonothermal events in the region. Apart from the helium potentiality in the EAHP, heat flow anomaly presents a proxy for geothermal energy targets.

The changes of heat flow anomalies in the Rukwa Rift that is, between 64 and 99 mW/m^2 are marked by corresponding changes in topographic profile. The RRB is a potential setting for radiogenic helium accumulation, however, the presence of other factors such as trapping and preservation of the accumulated helium are crucial for a potential helium resource.

Acknowledgements This work was funded by United Kingdom Commonwealth Scholarship Commission, the results of which is part of the first author's PhD study at the Durham University.

Author contributions Ernest Mulaya: conceptualization, methodology, formal analysis, modelling, writing—original draft, writing—review and editing; Jon Gluyas: funding acquisition, designed the research framework, supervision, review and editing; Ken McCaffrey: funding acquisition, designed the research framework, supervision, review and editing; David Byrne: provided geochemistry context and conceptualization; Chris Ballentine: assisted in funding acquisition and supervision.

Declarations

Conflict of interest The authors declare no conflicts of interest that are relevant to the content of this article.

References

Adams JAS, Osmond JK, Rogers JJW (1959) The geochemistry of thorium and uranium. Phys Chem Earth 3:298–348. https://doi.org/10.1016/0079-1946(59)90008-4

Andersen LS, Unrug R (1984) Geodynamic evolution of the Bangweulu Block, northern Zambia. Precambrian Res 25(1–3):187–212. https://doi.org/10.1016/0301-9268(84)90032-9

Barry PH, Hilton DR, Fischer TP, de Moor JM, Mangasini F, Ramirez C (2013) Helium and carbon isotope systematics of cold "mazuku" CO_2 vents and hydrothermal gases and fluids from Rungwe Volcanic Province, southern Tanzania. Chem Geol 339:141–156. https://doi.org/10.1016/j.chemgeo.2012.07.003

Bellahsen N, Husson L, Autin J, Leroy S, d'Acremont E (2013) The effect of thermal weakening and buoyancy forces on rift localization: field evidences from the Gulf of Aden oblique rifting. Tectonophysics 607:80–97. https://doi.org/10.1016/j.tecto.2013.05.042

Boniface N (2009) Eburnian, Kibaran and Pan-African metamorphic events in the Ubendian belt of Tanzania: Petrology, zircon and monazite geochronology (PhD dissertation). Kiel University, Germany

Boniface N (2017) Crystal chemistry of pyrochlore from the Mesozoic Panda Hill carbonatite deposit, western Tanzania. J Afr Earth Sci 126:33–44. https://doi.org/10.1016/j.jafrearsci.2016.11.026

Boniface N, Schenk V (2012) Neoproterozoic eclogites in the Paleoproterozoic ubendian belt of Tanzania: evidence for a pan-African suture between the bangweulu block and the Tanzania craton. Precambrian Res 208:72–89. https://doi.org/10.1016/j.precamres.2012.03.014

Borrego D, Nyblade AA, Accardo NJ, Gaherty JB, Ebinger CJ, Shillington DJ, Chindandali PR, Mbogoni G, Ferdinand RW, Mulibo G, O'Donnell JP, Kachingwe M, Tepp G (2018) Crustal structure surrounding the northern Malawi rift and beneath the Rungwe volcanic province. East Africa Geophys J Int 215(2):1410–1426. https://doi.org/10.1093/gji/ggy331

Brevart O, Dupre B, Allegre CJ (1982) Metallogenic provinces and the remobilization process studied by lead isotopes; lead-zinc ore deposits from the southern Massif Central. France Econ Geol 77(3):564–575. https://doi.org/10.2113/gsecongeo.77.3.564

Brown RJ, Manya S, Buisman I, Fontana G, Field M, Mac Niocaill C, Sparks RSJ, Stuart FM (2012) Eruption of kimberlite magmas: physical volcanology, geomorphology and age of the youngest kimberlitic volcanoes known on earth (the Upper Pleistocene/Holocene Igwisi Hills volcanoes, Tanzania). Bull Volcanol 74(7):1621–1643. https://doi.org/10.1007/s00445-012-0619-8

Bulanova GP, Muchemwa E, Pearson DG, Griffin BJ, Kelley SP, Klemme S, Smith CB (2004) Syngenetic inclusions of yimengite in diamond from Sese kimberlite (Zimbabwe): evidence for metasomatic conditions of growth. Lithos 77(1–4):181–192. https://doi.org/10.1016/j.lithos.2004.04.002

Burwash RA, Cumming GL (1976) Uranium and thorium in the Precambrian basement of western Canada I Abundance and distribution. Can J Earth Sci 13(2):284–293

Chaki S, Takarli M, Agbodjan WP (2008) Influence of thermal damage on physical properties of a granite rock: porosity, permeability and ultrasonic wave evolutions. Constr Build Mater 22(7):1456–1461. https://doi.org/10.1016/j.conbuildmat.2007.04.002

Chapman DS, Pollack HN (1975) Global heat flow: a new look. Earth Planet Sci Lett 28(1):23–32. https://doi.org/10.1016/0012-821X(75)90069-2

Cheng A, Lollar BS, Warr O, Ferguson G, Idiz E, Mundle SO, Barry PH, Byrne DJ, Mabry JC, Ballentine CJ (2021) Determining the role of diffusion and basement flux in controlling 4He distribution in sedimentary basin fluids. Earth Planet Sci Lett 2021 574:117175. https://doi.org/10.1016/j.epsl.2021.117175

Curtis GH, Reynolds JH (1958) Notes on the potassium-argon dating of sedimentary rocks. Geol Soc America Bull 69(2):151. https://doi.org/10.1130/0016-7606(1958)69[151:notpdo]2.0.co;2

Daly MC (1988) Crustal shear zones in central Africa: a kinematic approach to Proterozoic tectonics. Episodes 11(1):5–11. https://doi.org/10.18814/epiiugs/1988/v11i1/003

Danabalan D, Gluyas JG, Macpherson CG, Abraham-James TH, Bluett JJ, Barry PH, Ballentine CJ (2022) The principles of helium exploration. Petroleum Geosci. https://doi.org/10.1144/petgeo2021-029

Danabalan D (2017) Helium: Exploration methodology for a strategic resource (PhD thesis). Durham University, UK. pp1–293.

Davis WJ, Villeneuve ME (2001) Evaluation of the ^{232}Th decay constant by empirical cross-calibration of ^{208}Pb/^{232}Th and ^{207}Pb/^{235}U systematics in monazites. (Abs. #3838) 11th Annual V.M. Goldschmidt Conference, Hot Springs, Virginia, USA (2001).

Delvaux D (2001) Karoo rifting in western Tanzania: precursor of Gondwana break-up, contributions to geology and paleontology of Gondwana in honor of Helmut Wopfner. University of Cologne, Germany, Geological Institute, pp 111–125

Didas MM, Armadillo E, Hersir GP, Cumming W, Rizzello D (2022) Regional thermal anomalies derived from magnetic spectral analysis and 3D gravity inversion: implications for potential geothermal sites in Tanzania. Geothermics 103:102431. https://doi.org/10.1016/j.geothermics.2022.102431

Ebinger CJ, Sleep NH (1998) Cenozoic magmatism throughout east Africa resulting from impact of a single plume. Nature 395(6704):788–791. https://doi.org/10.1038/27417

Ebinger CJ, Deino AL, Drake RE, Tesha AL (1989) Chronology of volcanism and rift basin propagation: rungwe volcanic province East Africa. J Geophys Res 94(B11):15785–15803. https://doi.org/10.1029/jb094ib11p15785

Ebinger CJ, van Wijk J, Keir D (2013) The time scales of continental rifting: Implications for global processes. In: (Bickford ME ed) The web of geological sciences: advances, impacts, and interactions. Geological Society of America. pp 371–396. https://doi.org/10.1130/2013.2500(11)

Fritz H, Abdelsalam M, Ali KA, Bingen B, Collins AS, Fowler AR, Ghebreab W, Hauzenberger CA, Johnson PR, Kusky TM, Macey P, Muhongo S, Stern RJ, Viola G (2013) Orogen styles in the east African Orogen: a review of the Neoproterozoic to Cambrian tectonic evolution. J Afr Earth Sci 86:65–106. https://doi.org/10.1016/j.jafrearsci.2013.06.004

Gluyas JG (2019a) The emergence of the helium industry: The history of helium exploration, part 1 of 2. American association of petroleum geologists explorer. January 2019, 16–17.

Gluyas JG (2019b) Helium shortages and emerging helium provinces: The history of helium exploration (Part 2). American association of petroleum geologists explorer. February 2019, 18–22.

Halford DT, Karolytė R, Barry PH, Whyte CJ, Darrah TH, Cuzella JJ, Sonnenberg SA, Ballentine CJ (2022) High helium reservoirs in the four corners area of the Colorado Plateau, USA. Chem Geol 596:120790. https://doi.org/10.1016/j.chemgeo.2022.120790

Harkin DA (1960) The Rungwe Volcanics at the northern end of Lake Nyasa.

Holland G, Lollar BS, Li L, Lacrampe-Couloume G, Slater GF, Ballentine CJ (2013) Deep fracture fluids isolated in the crust since

the Precambrian era. Nature 497(7449):357–360. https://doi.org/10.1038/nature12127
Hu SB, He LJ, Wang JY (2000) Heat flow in the continental area of China: a new data set. Earth Planet Sci Lett 179(2):407–419. https://doi.org/10.1016/S0012-821X(00)00126-6
Ingebritsen SE, Manning CE (2010) Permeability of the continental crust: dynamic variations inferred from seismicity and metamorphism. Geofluids 10(1–2):193–205. https://doi.org/10.1111/j.1468-8123.2010.00278.x
James TC (1967) Thermal springs in Tanzania. Inst Min Metall Trans Sect B 76:B1–B18
Jones DJR (2020) A summary of the East Africa Rift temperature and heat flow model (Earth). BGS Open Report, OR/20/006
Kachingwe M, Nyblade A, JuliÀ J (2015) Crustal structure of Precambrian terranes in the southern African subcontinent with implications for secular variation in crustal genesis. Geophys J Int 202(1):533–547. https://doi.org/10.1093/gji/ggv136
Kilembe EA, Rosendahl BR (1992) Structure and stratigraphy of the Rukwa Rift. Tectonophysics 209(1–4):143–158. https://doi.org/10.1016/0040-1951(92)90016-Y
Kimani CN, Kasanzu CH, Tyne RL, Mtili KM, Byrne DJ, Kazimoto EO, Hillegonds DJ, Ballentine CJ, Barry PH (2021) He, Ne, Ar and CO_2 systematics of the Rungwe Volcanic province, Tanzania: implications for fluid source and dynamics. Chem Geol 586:120584. https://doi.org/10.1016/j.chemgeo.2021.120584
Kolawole F, Phillips TB, Atekwana EA, Jackson CA (2021) Structural inheritance controls strain distribution during early continental rifting, rukwa rift. Front Earth Sci 9:707869. https://doi.org/10.3389/feart.2021.707869
Koptev A, Calais E, Burov E, Leroy S, Gerya T (2015) Dual continental rift systems generated by plume–lithosphere interaction. Nat Geosci 8(5):388–392. https://doi.org/10.1038/ngeo2401
Last R, Nyblade A, Langston C, Owens T (1997) Crustal structure of the east African Plateau from receiver functions and Rayleigh wave phase velocities. J Geophys Res (Solid Earth) 102:24469–24483. https://doi.org/10.1029/97JB02156
Lavayssière A, Drooff C, Ebinger C, Gallacher R, Illsley-Kemp F, Oliva SJ, Keir D (2019) Depth extent and kinematics of faulting in the southern Tanganyika Rift. Africa Tectonics 38(3):842–862. https://doi.org/10.1029/2018tc005379
Lee H, Muirhead JD, Fischer TP, Ebinger CJ, Kattenhorn SA, Sharp ZD, Kianji G (2016) Massive and prolonged deep carbon emissions associated with continental rifting. Nat Geosci 9:145–149. https://doi.org/10.1038/ngeo2622
Lemna OS, Stephenson R, Cornwell DG (2019) The role of pre-existing Precambrian structures in the development of Rukwa Rift Basin, southwest Tanzania. J Afr Earth Sci 150:607–625. https://doi.org/10.1016/j.jafrearsci.2018.09.015
Lenoir JL, Liégeois JP, Theunissen K, Klerkx J (1994) The Palaeoproterozoic ubendian shear belt in Tanzania: geochronology and structure. J Afr Earth Sci 19(3):169–184. https://doi.org/10.1016/0899-5362(94)90059-0
Lowenstern JB, Evans WC, Bergfeld D, Hunt AG (2014) Prodigious degassing of a billion years of accumulated radiogenic helium at Yellowstone. Nature 506(7488):355–358. https://doi.org/10.1038/nature12992
Lysak SV (1992) Heat flow variations in continental rifts. Tectonophysics 208(1–3):309–323. https://doi.org/10.1016/0040-1951(92)90352-7
Manya S, Maboko MAH, Nakamura E (2007) The geochemistry of high-Mg andesite and associated adakitic rocks in the Musoma-Mara Greenstone Belt, northern Tanzania: Possible evidence for Neoarchaean ridge subduction? Precambrian Res 159(3–4):241–259. https://doi.org/10.1016/j.precamres.2007.07.002
Mareschal JC, Gliko A (1991) Lithospheric thinning, uplift, and heat flow preceding rifting. Tectonophysics 197(2–4):117–126. https://doi.org/10.1016/0040-1951(91)90036-R
Morley CK,Wescott WA, Harper RM, Cunningham SM (1999) Geology and geophysics of the Rukwa Rift. In: (C.K.Morley ed.) Geoscience of rift systems—Evolution of East Africa. American Association of Petroleum Geologists, pp 91–110. https://doi.org/10.1306/st44623c5
Mshiu EE, Maboko MAH (2012) Geochemistry and petrogenesis of the late Archaean high-K granites in the southern Musoma-Mara Greenstone Belt: their influence in evolution of Archaean Tanzania Craton. J Afr Earth Sci 66:1–12. https://doi.org/10.1016/j.jafrearsci.2012.03.002
Mtili KM, Byrne DJ, Tyne RL, Kazimoto EO, Kimani CN, Kasanzu CH, Hillegonds DJ, Ballentine CJ, Barry PH (2021) The origin of high helium concentrations in the gas fields of southwestern Tanzania. Chem Geol 585:120542. https://doi.org/10.1016/j.chemgeo.2021.120542
Mulaya E, Gluyas J, McCaffrey K, Phillips T, Ballentine C (2022) Structural geometry and evolution of the rukwa rift basin, Tanzania: implications for helium potential. Basin Res 34(2):938–960. https://doi.org/10.1111/bre.12646
Negredo AM, Fernàndez M, Zeyen H (1995) Thermo-mechanical constraints on kinematic models of lithospheric extension. Earth Planet Sci Lett 134(1–2):87–98. https://doi.org/10.1016/0012-821X(95)00107-N
Njinju EA, Kolawole F, Atekwana EA, Stamps DS, Atekwana EA, Abdelsalam MG, Mickus KL (2019) Terrestrial heat flow in the Malawi Rifted zone, east Africa: Implications for tectonothermal inheritance in continental rift basins. J Volcanol Geotherm Res 387:106656. https://doi.org/10.1016/j.jvolgeores.2019.07.023
Park Y, Nyblade AA (2006) P-wave tomography reveals a westward dipping low velocity zone beneath the Kenya Rift. Geophys Res Lett. https://doi.org/10.1029/2005GL025605
Parsons-Davis T, Wimpenny J, Keller CB, Thomas K, Samperton KM, Renne PR, Mundil R, Moody K, Knight K, Kristo MJ, Williams R (2018) New measurement of the ^{238}U decay constant with inductively coupled plasma mass spectrometry. J Radioanal Nucl Chem 318(1):711–721. https://doi.org/10.1007/s10967-018-6148-y
Pik R, Marty B, Hilton DR (2006) How many mantle plumes in Africa? The geochemical point of view. Chem Geol 226(3–4):100–114. https://doi.org/10.1016/j.chemgeo.2005.09.016
Pinna P, Calvez JY, Abessolo A, Angel JM, Mekoulou-Mekoulou T, Mananga G, Vernhet Y (1994) Neoproterozoic events in the Tcholliré area: Pan-African crustal growth and geodynamics in central-northern Cameroon (Adamawa and north provinces). J Afr Earth Sci 18(4):347–353. https://doi.org/10.1016/0899-5362(94)90074-4
Plasman M, Tiberi C, Ebinger C, Gautier S, Albaric J, Peyrat S, Déverchère J, Le Gall B, Tarits P, Roecker S, Wambura F, Muzuka A, Mulibo G, Mtelela K, Msabi M, Kianji G, Hautot S, Perrot J, Gama R (2017) Lithospheric low-velocity zones associated with a magmatic segment of the Tanzanian Rift. East Africa Geophys J Int 210(1):465–481. https://doi.org/10.1093/gji/ggx177
Pollack HN (1982) The heat flow from the continents. Annu Rev Earth Planet Sci 10:459–481. https://doi.org/10.1146/annurev.ea.10.050182.002331
Polyak BG, Smirnov YB (1968) Relationship between terrestrial heat flow and the tectonics of continents. Geotectonics 4:205–213
Quennell AM, McKinlay AC, Aitken WG (1956) Summary of the geology of Tanganyika, part 1. Geological Surv. Tanganyika Mem. pp126.
René M (2017) Nature, sources, resources, and production of thorium. In: descriptive inorganic chemistry researches of metal compounds. https://doi.org/10.5772/intechopen.68304

Sclater JG, Jaupart C, Galson D (1980) The heat flow through oceanic and continental crust and the heat loss of the Earth. Rev Geophys Space Phys 18:269–311. https://doi.org/10.1029/RG018i001p00269

Shirey SB, Cartigny P, Frost DJ, Keshav S, Nestola F, Nimis P, Pearson DG, Sobolev NV, Walter MJ (2013) Diamonds and the geology of mantle carbon. Rev Mineral Geochem 75(1):355–421. https://doi.org/10.2138/rmg.2013.75.12

Stamps DS, Saria E, Kreemer C (2018) A geodetic strain rate model for the east African Rift system. Sci Rep 8(1):732. https://doi.org/10.1038/s41598-017-19097-w

Stiefenhofer J, Farrow DJ (2004) Geology of the Mwadui kimberlite, Shinyanga district. Tanzania Lithos 76(1–4):139–160. https://doi.org/10.1016/j.lithos.2004.04.017

Taylor RE, Aitken MJ (1997) Chronometric dating in archaeology. Springer US, https://doi.org/10.1007/978-1-4757-9694-0

Theunissen K, Klerkx J, Melnikov A, Mruma A (1996) Mechanisms of inheritance of rift faulting in the western branch of the East African Rift Tanzania. Tectonics 15(4):776–790. https://doi.org/10.1029/95tc03685

Torgersen T (2010) Continental degassing flux of 4 He and its variability. Geochem Geophys Geosyst. https://doi.org/10.1029/2009GC002930

Warr O, Sherwood Lollar B, Fellowes J, Sutcliffe CN, McDermott JM, Holland G, Mabry JC, Ballentine CJ (2018) Tracing ancient hydrogeological fracture network age and compartmentalisation using noble gases. Geochim Cosmochim Acta 222:340–362. https://doi.org/10.1016/j.gca.2017.10.022

Weeraratne DS, Forsyth DW, Fischer KM, Nyblade AA (2003) Evidence for an upper mantle plume beneath the Tanzanian craton from Rayleigh wave tomography. J Geophys Res: Solid Earth. https://doi.org/10.1029/2002JB002273

Wetherill GW, Wasserburg GJ, Aldrich LT, Tilton GR, Hayden RJ (1956) Decay constants of K40 as determined by the radiogenic argon content of potassium minerals. Phys Rev 103(4):987–989. https://doi.org/10.1103/PhysRev.103.987

Wilks M, Kendall JM, Nowacki A, Biggs J, Wookey J, Birhanu Y, Ayele A, Bedada T (2017) Seismicity associated with magmatism, faulting and hydrothermal circulation at Aluto Volcano, Main Ethiopian Rift. J Volcanol Geotherm Res 340:52–67. https://doi.org/10.1016/j.jvolgeores.2017.04.003